NACA RM A55L02

NACA

RESEARCH MEMORANDUM

EFFECT OF BOUNDARY-LAYER CONTROL AND INLET LIP SHAPE ON THE PERFORMANCE OF A TWIN-SCOOP AIR-INDUCTION SYSTEM AT MACH NUMBERS FROM 0 TO 1.9

By Frank A. Lazzeroni and Frank A. Pfyl

Ames Aeronautical Laboratory
Moffett Field, Calif.

NATIONAL ADVISORY COMMITTEE
FOR AERONAUTICS

WASHINGTON

February 14, 1956
Declassified August 19, 1960

NATIONAL ADVISORY COMMITTEE FOR AERONAUTICS

RESEARCH MEMORANDUM

EFFECT OF BOUNDARY-LAYER CONTROL AND INLET LIP SHAPE ON THE PERFORMANCE OF A TWIN-SCOOP AIR-INDUCTION SYSTEM AT MACH NUMBERS FROM 0 TO 1.9

By Frank A. Lazzeroni and Frank A. Pfyl

SUMMARY

An experimental investigation was conducted to determine the effect of boundary-layer control and inlet lip shape on the performance of a side-inlet air-induction system for a fighter-type airplane. Two methods of boundary-layer control were investigated, one which allowed the low-energy air to pass under a compression ramp placed one boundary-layer height away from the fuselage and the other in which a portion of the low-energy air was drawn off through a permeable compression ramp placed contiguous to the fuselage surface. Three inlet lip shapes of varying degrees of bluntness were also investigated. Tests were made at Mach numbers from 0 to 1.9 at an angle of attack of 4° and mass-flow ratios from 0 to the maximum obtainable.

The results indicated that boundary-layer control had a favorable effect on the total pressure recovery and inlet air-flow steadiness of the inlets tested. However, boundary-layer control resulted in an increase in drag for each configuration tested. A comparison of the two types of boundary-layer control systems investigated showed that, in general, the system in which the low-energy air was allowed to pass under the compression ramp had higher net propulsive thrust and a larger stable range of operation than the system in which low energy air was drawn off through a permeable compression ramp.

At the supersonic and high subsonic speeds of the tests, only small differences in total pressure recovery existed between the three lip shapes investigated. However, at the simulated take-off condition, the blunt-lip inlet showed a considerable increase in pressure recovery over both the thin-lip and sharp-lip inlets. Although no significant differences in net propulsive thrust existed between the thin-lip and sharp-lip inlets at supersonic speeds, both had somewhat higher net propulsive thrust than the blunt-lip inlet.

It was noted for all inlets tested that as the mass-flow ratio was reduced below its maximum, a value was reached at which flow asymmetry occurred such that the inlet on one side of the fuselage operated at a higher mass-flow ratio than the inlet on the other side.

INTRODUCTION

Recent studies on boundary-layer control systems for side-inlet air-induction systems, references 1 through 3, have shown that the pressure recovery and drag are strongly influenced by the design details in the vicinity of the inlet entrance. Generally, the effects on pressure recovery and drag of controlling the boundary-layer air depend on the particular inlet-fuselage combination and, with the exception of a few cases, comparisons between air-induction systems utilizing various methods of boundary-layer control and these systems with the boundary-layer air allowed to enter the inlet have not been made. Additional comparisons for a variety of configurations are necessary if the designer is to determine whether, for a new inlet, the increase in pressure recovery due to efficient boundary-layer control will overbalance the increase in drag and the inherent penalties associated with the added structure, weight, and design complexities of these systems. In this report performance data for several inlet configurations are presented and evaluated. The drag, air-flow unsteadiness, pressure recovery, and mass-flow characteristics of a particular inlet and fuselage combination having two different methods of boundary-layer control were investigated. The performance of each configuration was compared analytically by means of a net thrust parameter with an equivalent air-inlet configuration without boundary-layer removal. The methods of boundary-layer control investigated were a wedge-diverter system for which the inlet and compression ramp were placed one boundary-layer height from the fuselage surface allowing the low-energy air to pass under the compression ramp, and a suction system which removed a portion of the low-energy air through a permeable compression ramp placed contiguous to the fuselage surface. In addition, an investigation was made to evaluate the effect of lip shape on the inlet with the compression ramp placed one boundary-layer height from the fuselage surface.

SYMBOLS

A area, sq ft

A_{min} minimum internal diffuser cross-sectional area (fuselage station 19.10), sq ft

$\frac{A_{min}}{A_i}$ contraction ratio

C_D net drag coefficient, $\frac{D}{qS}$

D net drag, lb

h boundary-layer diverter height from fuselage surface, in.

$\frac{h}{\delta}$ boundary-layer thickness parameter

M Mach number

m_c mass flow through inlet (measured at compressor station), slugs/sec

$\frac{m_c}{m_\infty}$ ratio of the mass flow through the inlet to the mass flow at the free-stream conditions passing through an area equal to the inlet entrance area, $\frac{\rho_c A_c V_c}{\rho_\infty A_i V_\infty}$

p static pressure, lb/sq ft

p_t total pressure, lb/sq ft

$\frac{p_{t_c}}{p_{t_\infty}}$ total-pressure ratio at the compressor station

Δp pressure difference across porous compression surface, lb/sq in.

q dynamic pressure, lb/sq ft

R Reynolds number

S wing area, 8.703 sq ft

T_I net thrust with isentropic pressure recovery, lb

T_N net thrust with measured pressure recovery, lb

V velocity, ft/sec

$\frac{W_a\sqrt{\theta_c}}{A_i\delta_c}$ air-flow parameter, $\frac{\text{lb/sec}}{\text{sq ft}}$

W_a weight flow of air, lb/sec

α angle of attack of fuselage reference axis, deg

δ boundary-layer thickness (distance from fuselage surface to point in boundary layer where velocity is 0.99 local velocity), in.

δ_c compressor station total pressure divided by NACA sea-level static pressure

η net-thrust parameter, $\frac{T_N - D}{T_I}$

θ_c absolute total temperature at compressor station divided by NACA absolute ambient sea-level temperature

ρ mass density of air, slugs/cu ft

Subscripts

c compressor station

i inlet entrance station (defined in fig. 3)

∞ free-stream condition

APPARATUS AND PROCEDURE

The air-induction model shown in figure 1 was the same, except for the inlet region, as that for the investigation reported in reference 1 in which a detailed description of the instrumentation, apparatus, and procedure may be found. The modifications made to the inlet region of the basic trapezoidal configuration to obtain models of the present investigation included changes to the boundary-layer removal system and to the lip contour. Two different methods for removing the boundary-layer air were tested on the model. One method utilized a sharp wedge underneath the inlet (see fig. 1 or 2(a)). The compression ramp was placed one boundary-layer height away from the fuselage ($h/\delta = 1.0$ at $M_\infty = 1.5$) to allow the fuselage boundary layer to pass under the compression ramp. This method of boundary-layer control will be referred to in the text as a diverter system. The other method, a suction type utilizing the pressure difference across the ramp, removed only the low-energy portion of the fuselage boundary layer through permeable compression surfaces placed contiguous to the fuselage surface (see fig. 2(c)). Two porous surfaces were used, one of sintered material and the other a porous ramp obtained by drilling 0.10-inch-diameter holes through a solid ramp surface. A solid ramp was also tested. For the porous type, the mass of air removed was calculated from total- and static-pressure data measured near the boundary-layer removal exit (see fig. 2(c) for view of

exit). The angle of the ramp compression surfaces for all removal systems was 7° relative to the fuselage center line. Three lip shapes were investigated in conjunction with the diverter-type boundary-layer removal system, and two lip shapes were tested with a solid ramp (no diverter). The lips are designated the blunt lip, thin lip, and sharp lip (leading-edge radii of 0.065, 0.025, and 0.015 inch, respectively) in the remainder of the text (see figs. 3(a) and 3(b)). The reference line for the thin and sharp lips (fig. 3(b)) is not the same as that for the blunt lip (fig. 3(a)).

A comparison of the boundary-layer systems and lip shapes can be made from the photographs of figure 2, and the various inlet configurations that were tested are listed in the following table:

Lip shape	Boundary-layer control system	Compression surface
1. Blunt	Diverter	Solid
2. Thin	Diverter	Solid
3. Sharp	Diverter	Solid
4. Blunt	None	Solid
5. Thin	None	Solid
6. Thin	Suction	Sintered steel material such that 1 percent of inlet mass flow could be drawn through surface ($\Delta p = 0.08\ p_{t_\infty}$)
7. Thin	Suction	Two hundred and ten 0.1-inch-diameter holes spaced on 0.2-inch centers

Shown in figures 4 to 7 are various details of the boundary-layer-wedge diverter, a schematic drawing of the survey rake and pressure cells, the lip coordinates and a sketch of each lip, the model area distribution, and the diffuser area variation up to the compressor inlet. The model instrumentation consisted of a survey rake at the simulated compressor inlet (see fig. 5) from which the internal air-flow forces and the air-induction parameters, pressure recovery and mass-flow ratio, were determined. Further instrumentation consisted of strain-gage-type pressure cells to measure the air-flow unsteadiness and a six-component strain-gage balance used to obtain the aerodynamic forces. To insure that the frictional forces would remain relatively constant, transition was fixed near the apex of the nose and near the leading edge of the lip of the inlets (see ref. 1).

The experimental investigation was conducted in the Ames 6- by 6-foot supersonic wind tunnel. A complete description of this wind tunnel may be found in reference 4.

Data were obtained through a range of mass-flow ratios from 0 to the maximum obtainable, at an angle of attack of 4°, and at Mach numbers of 0, 0.9, 1.3, 1.5, 1.7, and 1.9. Drag data are not presented at $M_{\infty} = 1.3$ since the reflection of the bow shock wave from the tunnel walls intersected the afterportion of the model. With the exception of the static tests ($M_{\infty} = 0$), all experimental data were obtained at a constant tunnel stagnation pressure of 10 pounds per square inch absolute. This corresponds to a Reynolds number (per foot) as shown in the following table:

M_{∞}	R, million
0.9	3.0
1.3	2.5
1.5	2.9
1.7	2.8
1.9	2.6

The estimated uncertainty introduced into each corrected dimensionless coefficient by the known uncertainties in the measurements are tabulated below:

Quantity	Uncertainty
C_D	± 0.0005
$p_{t_c}/p_{t_{\infty}}$	± 0.005
m_c/m_{∞}	± 0.01
M	± 0.03
R	$\pm 0.03 \times 10^6$
α	$\pm 0.15^{\circ}$

DISCUSSION

The present discussion has been divided into three main parts. The first part is concerned with the two types of boundary-layer control systems investigated, a diverter system and a porous suction system. The effect of these boundary-layer control systems on the total pressure recovery, drag, and air-flow steadiness of the inlets is presented. The second part compares the three inlet lip shapes that were tested on the basis of total pressure recovery and drag. The third section presents a comparison of the various boundary-layer control systems and inlet lip shapes investigated on the basis of a net thrust parameter.

Effect of Boundary-Layer Control Systems

Pressure recovery.- Previous experiments (ref. 2) have shown that in the Mach number range from 1.5 to 2.0, the use of a boundary-layer control system in which the low-energy air was allowed to pass under a splitter plate in front of a half-cone side inlet resulted in as much as a 25-percent increase in total pressure recovery over the same inlet with no boundary-layer control. Comparing the total pressure recovery of the present inlets with and without the diverter system (fig. 8, blunt lip, and fig. 9, thin lip) showed that the use of this type of boundary-layer control increased the pressure recovery from 3 to 5 percent throughout the supersonic speed range of the investigation. The large difference between the increase in pressure recovery obtained with the present diverter system and that of reference 2 is due to the fact that the total pressure recovery of the present system without the diverter was from 14 to 20 percent higher than that for the half-cone configuration without boundary-layer control, so that less gain is possible in the present case. The influence of the diverter on the flow field in front of the inlet, in the present installation, is illustrated in the schlieren photographs of figure 10.

Removing boundary-layer air through a porous compression surface in front of the inlet alwo increased the pressure recovery, but not as much as the diverter (compare figs. 9 and 11). Although the diverter gave the best pressure recovery of the boundary-layer control systems investigated, better results might be anticipated for the inlets utilizing porous compression surfaces if more air were removed through the porous surface. The amount of air removed through the sintered surface was from 2 to 2-1/2 percent of the inlet mass flow while 2-1/2 to 3-1/2 percent was removed through the surface with the 0.1-inch-diameter holes. (For comparison purposes the amount of air that passed under the compression ramp with the diverter system was estimated to be about 15 percent of the inlet mass flow at $M_\infty = 1.5$ and $m_c/m_\infty = 1.0$. This estimate was made by using the boundary-layer thickness as determined from schlieren photographs and the ratio of displacement thickness to total thickness given in reference 5 for a 1/7 power velocity profile.) Data in figure 11 show that with just the small amount of low-energy air removed through the permeable surfaces, gains in pressure recovery over that for the solid-ramp configuration ranged between 1 and 4 percent.

Drag.- Improving the pressure recovery of the inlets investigated by removing the fuselage boundary layer ahead of the inlets was accompanied by increases in drag due to the boundary-layer control systems used. From the results presented in figures 8 and 9, the increase in drag, with the system which allowed the low-energy air to pass under the compression ramp, was from 5 to 9 percent of the total drag of the model in the Mach number range from 1.5 to 1.9. If a total drag coefficient of 0.0235 is assumed for an airplane in high-speed flight ($M_\infty = 1.5$) (having the present inlet-fuselage combination), the drag of the present system with

the diverter would be about 4 percent of the total drag of the airplane. For comparison, it has been calculated that the drag of various boundary-layer control systems of this type on typical interceptor aircraft represent from 3 to 10 percent of the total drag of the airplane.

Utilizing the porous compression surfaces as a means of removing the low-energy air from in front of the inlet resulted in drag increases up to 10 percent in the Mach number range from 1.5 to 1.9 (fig. 11). The major part of the drag of these boundary-layer control systems was associated with the design of the exit of the boundary-layer control duct, since calculations based on static- and total-pressure measurements in this duct showed that the drag due to the loss of momentum of the boundary-layer air in passing through the ducting system was small. At Mach numbers of 1.5 and 1.7 the drag of the inlet with the sintered compression surface was about 4 percent lower than the drag of the inlet with the 0.1-inch-diameter holes in the compression surface.

Inlet air-flow unsteadiness.- In the present air-induction systems there were pressure oscillations in the duct for all inlet configurations. The maximum total amplitude of these pressure oscillations, measured by the pressure cells in the ducting system, was used to indicate the relative degree of unsteadiness of the flow in the inlets investigated. The results presented in figure 12 (blunt lip) and figure 13 (thin lip) show that, in general, the inlets utilizing the boundary-layer diverter exhibited lower oscillation amplitudes over a wider mass-flow range, that is, larger stable range of operation than either the inlets without boundary-layer control or the inlets with porous compression surfaces. The reversal of trends shown at $M_\infty = 1.5$ in figure 12(c) is not understood.

It has been noted in previous experiments (ref. 1) that as the mass-flow ratio was reduced below its maximum, a value was reached at which flow asymmetry occurred such that the inlet on one side of the fuselage operated at a higher mass-flow ratio than the inlet on the other side. (This value of mass-flow ratio varied with M_∞ and with inlet configuration.) A similar flow condition occurred in the present investigation (see fig. 10). Flow asymmetry coincided with the rapid increase in the amplitude of the pressure pulsations as shown in figures 12 and 13. Also, the inlet with the higher mass flow had the lower amplitudes of pressure oscillations. This was observed from the difference between pressure oscillations of each duct (data shown for right duct only). A similar phenomenon has been observed in other side-inlet installations both at subsonic (ref. 6) and supersonic speeds (ref. 7) where the ducting from two inlets join in a common chamber.

Representative total-pressure contour maps at the simulated compressor entrance are presented (fig. 14) for the thin-lip inlet configurations at a typical operating condition for an inlet-engine combination ($M_\infty = 1.5$, $(m_c/m_\infty) \approx 0.90$). Observations of these maps and contour maps for other operating conditions (not shown) showed that, in general, the diverter

system had less radial and circumferential total-pressure distortion than any of the other inlets investigated. Although no contour maps are presented which show the effects of lip shape, no significant differences in radial and circumferential total-pressure distributions existed between these inlets and the thin-lip inlets at comparable test conditions. For all configurations tested, the lowest total pressure recovery at the compressor station occurred in the lower part of the duct. It is believed that this low-pressure region for angles of attack above about 4° is associated with a flow disturbance caused by the lower lip of the inlet.

Effect of Lip Shape

The three inlet lip shapes investigated, blunt lip, thin lip, and sharp lip (fig. 3), were tested in conjunction with the diverter air-induction system.

Pressure recovery.- From the results presented in figure 15 it is evident that the effect of lip shape on the inlet pressure recovery was small at the supersonic and high subsonic speeds of the tests. In general, however, the blunt-lip inlet had a slightly higher pressure recovery than either the thin-lip or sharp-lip inlets. At the simulated take-off condition ($M_{\infty} = 0$, fig. 16), the blunt-lip inlet had considerably higher pressure recovery than either the thin-lip or sharp-lip inlet. These results are similar to those obtained and reported in reference 8 where it was shown that blunting the inlet lip resulted in slight increases in pressure recovery at subsonic and supersonic speeds while comparatively large increases in pressure recovery were evidenced at the simulated take-off condition.

The sharp-lip inlet had higher pressure recovery than the thin-lip inlet at the simulated take-off condition (fig. 16). Since both lips had the same thickness aft of the lip region (fig. 3), it would appear that the pressure recovery was a function of the internal lip shape and contraction ratio at mass-flow ratios greater than 1.0.

Drag.- Net drag coefficients of the three lip shapes are presented as a function of mass-flow ratio in figure 15 for the test Mach numbers. These data show that the blunt lip had higher drag than the sharper lips throughout the supersonic speed range of the tests, while there was little difference in drag between the thin-lip and sharp-lip inlets. No drag differences existed between the three lip shapes at the high subsonic speed of the investigation.

Net Propulsive Thrust

A method of comparing the performance of the inlets consists of converting the drag force and pressure recovery into a single thrust parameter and comparing the inlets at their actual operating points. This performance analysis and the engine assumed in the calculations (the JT-3C-20) were the same as presented in reference 1.

The results of the analysis showed that the thin-lip inlet with the diverter-type boundary-layer control system had as high or higher net propulsive thrust than the remaining thin-lip inlet configurations throughout the Mach number range of the tests, except at $M_\infty = 0.9$ (fig. 17). It should be noted that only small differences in net thrust existed between the two types of boundary-layer control systems investigated. Any selection of a particular system might depend on other factors such as inlet air-flow stability and structural limitations. Of the three inlet lip shapes investigated (fig. 18), both the thin-lip and sharp-lip inlets had considerably higher net propulsive thrust than the blunt-lip inlet in the supersonic speed range. At the simulated take-off condition, however, the blunt-lip inlet had the highest net propulsive thrust of the three inlet shapes.

It can be seen that an inlet area of 4.2 square feet would be a good compromise for subsonic and supersonic operation up to $M_\infty = 1.5$. However, for operation at speeds above $M_\infty = 1.5$, a variable area inlet or an internal bypass system would be necessary for optimum operation.

CONCLUSIONS

The following conclusions were obtained from an investigation at Mach numbers from 0 to 1.9 of the effect of boundary-layer control and inlet lip shape on the performance of a side-inlet air-induction system for a fighter-type airplane:

1. Utilization of boundary-layer control resulted in a substantial increase in total pressure recovery throughout the speed range of the investigation.

2. The improvement in total pressure recovery by the use of boundary-layer control was accompanied by drag increases of up to 10 percent.

3. Inlet air-flow steadiness was generally improved by the use of boundary-layer control systems.

4. For all inlets investigated, when the mass-flow ratio was reduced below its maximum, a value was reached at which flow asymmetry occurred

such that the inlet on one side of the fuselage operated at a higher mass-flow ratio than the inlet on the other side. This value of mass-flow ratio varied with Mach number and inlet configuration.

5. In general, of the two types of boundary-layer control systems investigated, the one which utilized a diverter under the compression ramp and removed all the fuselage boundary-layer air from in front of the inlet had higher net propulsive thrust and a larger range of steady operation than the system in which only a portion of the low-energy air was drawn off through a permeable compression surface.

6. Effect of lip shape on total pressure recovery was small at the high subsonic and supersonic speeds of the tests. However, at the simulated take-off condition, the total pressure recovery obtained with the blunt-lip inlet showed a considerable increase over the thin-lip and sharp-lip inlets.

7. For all inlets investigated, the diverter system, in general, had less radial and circumferential total-pressure distortions at the simulated compressor entrance.

8. While no significant differences in net propulsive thrust existed between the thin-lip and sharp-lip inlets, both had somewhat higher net propulsive thrust than the blunt-lip inlet at supersonic speeds.

Ames Aeronautical Laboratory
National Advisory Committee for Aeronautics
Moffett Field, Calif., Dec. 2, 1955

REFERENCES

1. Mossman, Emmet A., Pfyl, Frank A., and Lazzeroni, Frank A.: Experimental Investigation at Mach Numbers from 0 to 1.9 of Trapezoidal and Circular Side Inlets for a Fighter-Type Airplane. NACA RM A55D27, 1955.

2. Valerino, Alfred S., Pennington, Donald B., and Vargo, Donald J.: Effect of Circumferential Location on Angle of Attack Performance of Twin Half-Conical Scoop-Type Inlets Mounted Symmetrically on the RM-10 Body of Revolution. NACA RM E53G09, 1953.

3. Campbell, Robert C., and Kremzier, Emil J.: Performance of Wedge-Type Boundary Layer Diverters for Side Inlets at Supersonic Speeds. NACA RM E54C23, 1954.

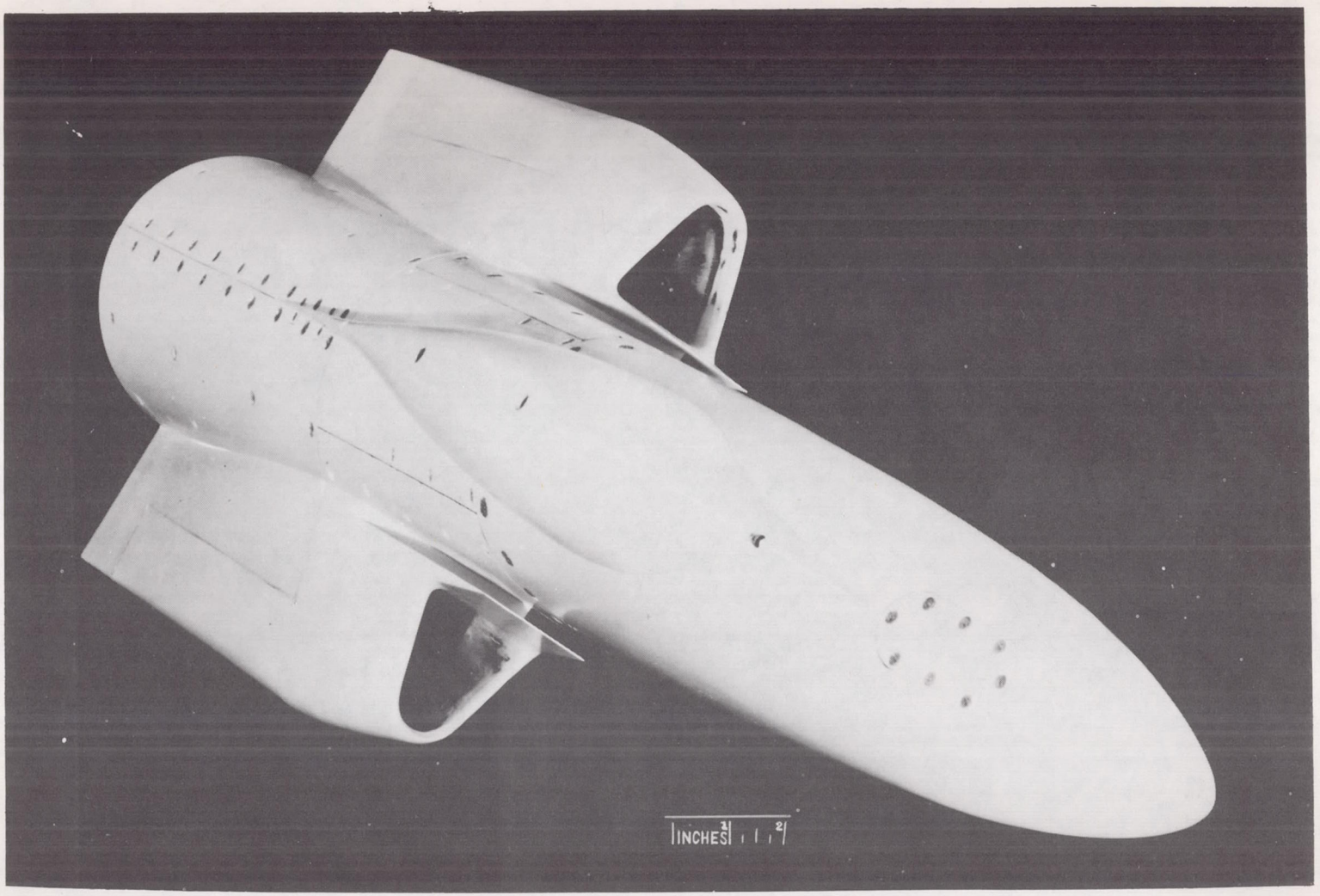
4. Frick, Charles W., and Olson, Robert N.: Flow Studies in the Asymmetric Adjustable Nozzle of the Ames 6- by 6-Foot Supersonic Wind Tunnel. NACA RM A9E24, 1949.

5. Tucker, Maurice: Approximate Calculation of Turbulent Boundary-Layer Development in Compressible Flow. NACA TN 2337, 1951.

6. Martin, Norman J., and Holzhauser, Curt A.: Analysis of Factors Influencing the Stability Characteristics of Symmetrical Twin-Intake Air-Induction Systems. NACA TN 2049, 1950.

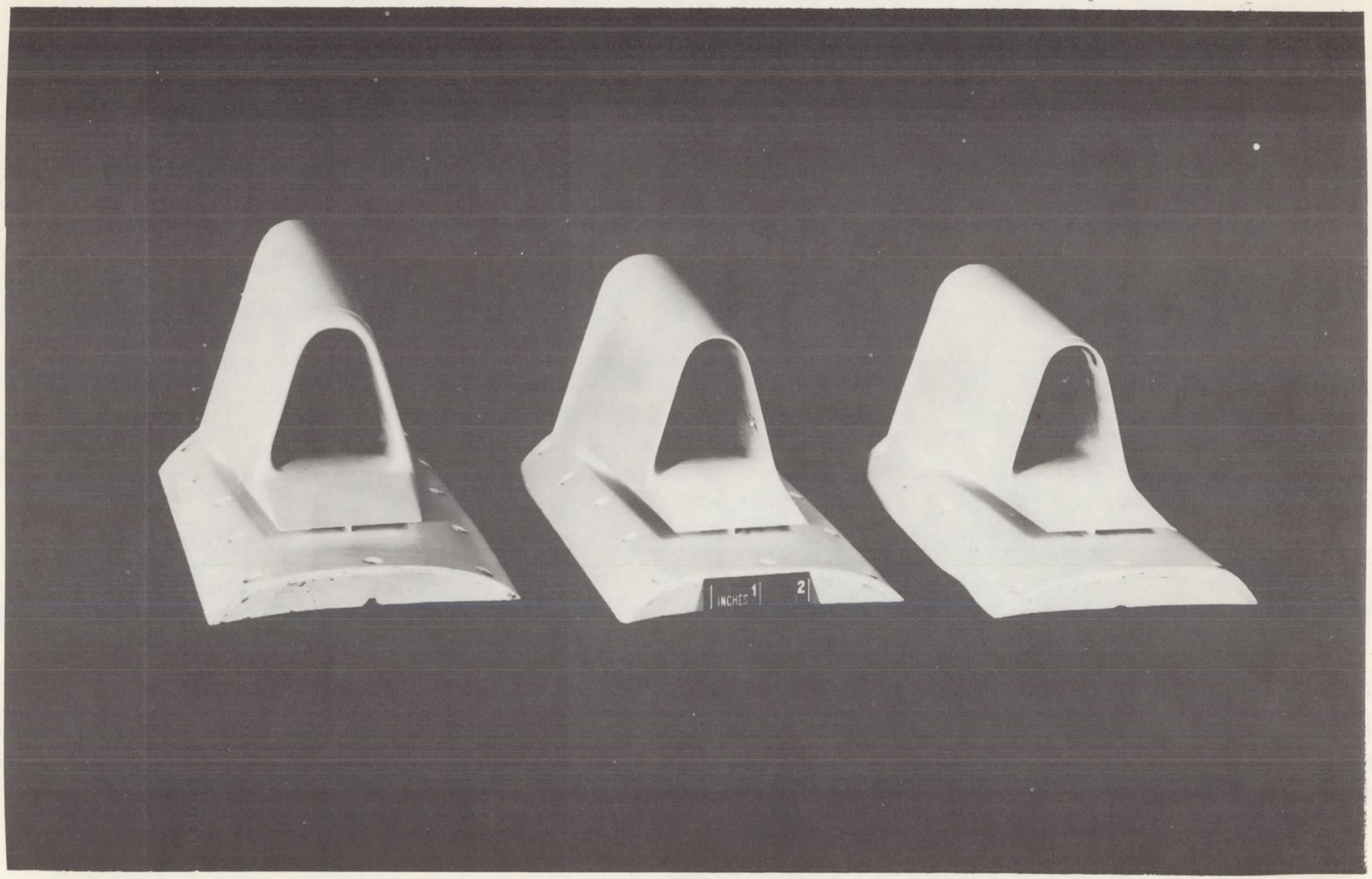
7. Davids, Joseph, and Wise, George A.: Investigation at Mach Numbers 1.5 and 1.7 of Twin-Duct Side Intake System with Two-Dimensional 6° Compression Ramps Mounted on a Supersonic Airplane. NACA RM E53H19, 1953.

8. Mossman, Emmet A., and Anderson, Warren E.: The Effect of Lip Shape on a Nose-Inlet Installation at Mach Numbers From 0 to 1.5 and a Method for Optimizing Engine-Inlet Combinations. NACA RM A54B08, 1954.



A-19399.2

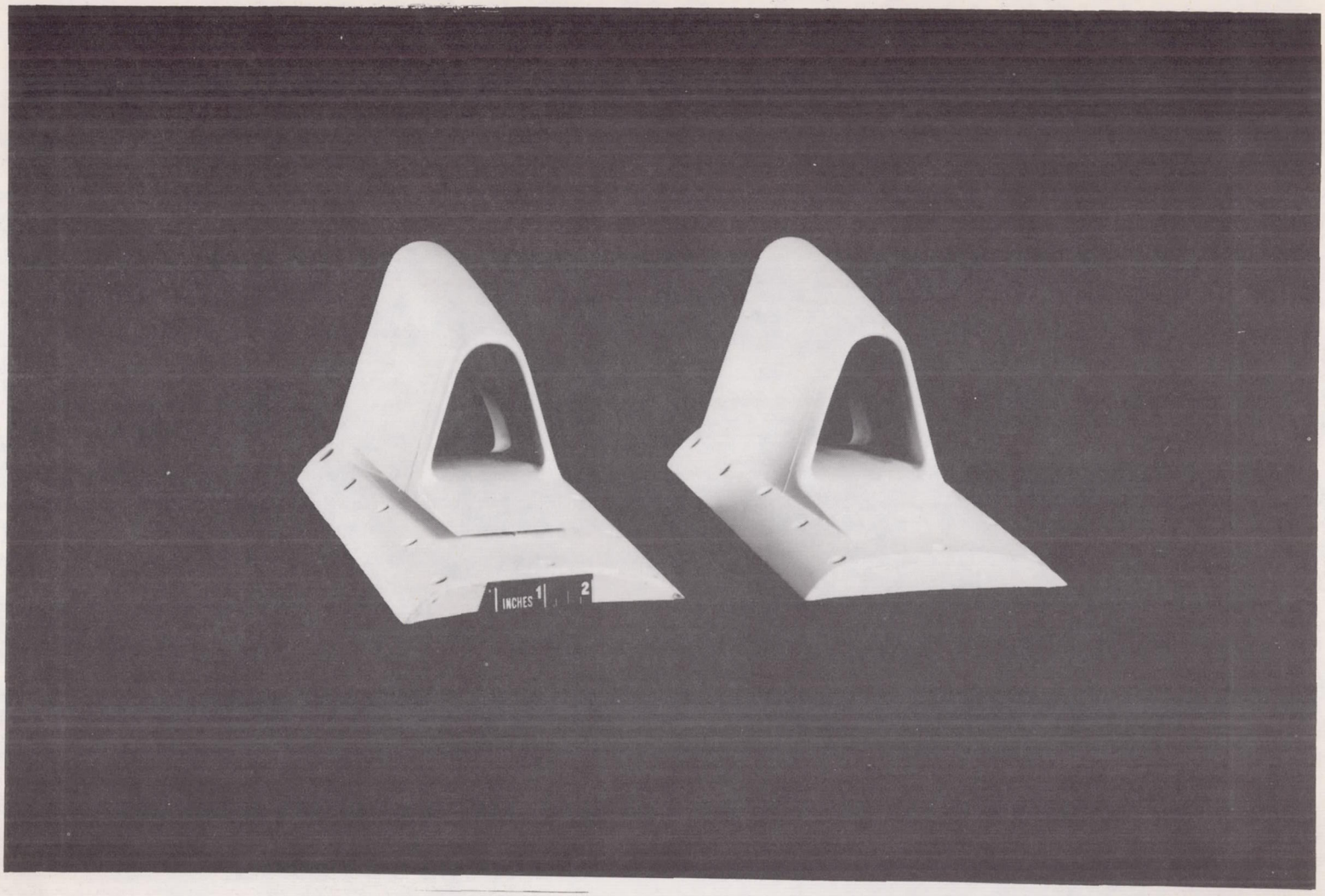
Figure 1.- Photograph of the air-induction model with the blunt-lip inlet and diverter boundary-layer control system.



A-20340

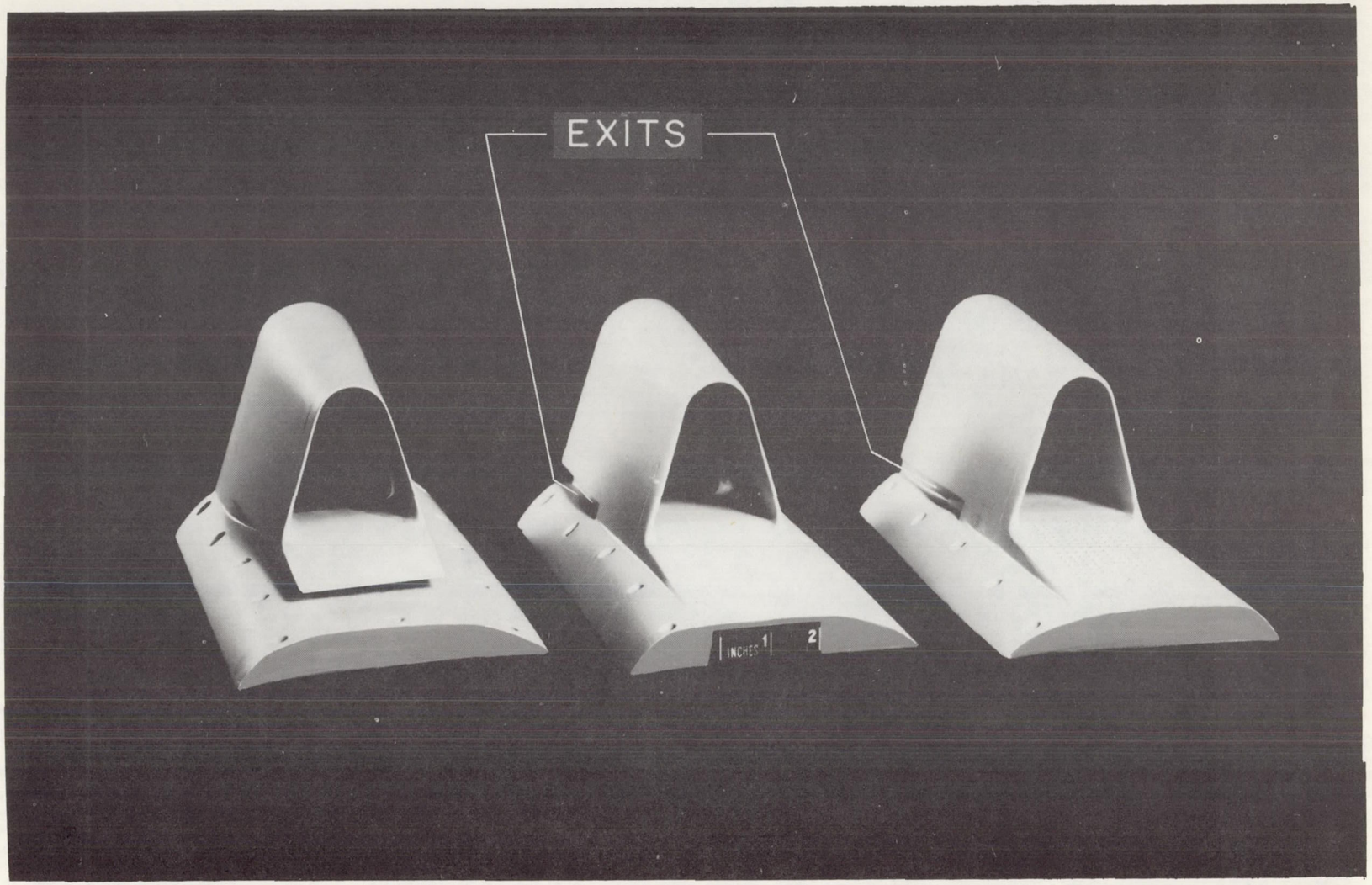
(a) Blunt lip, thin lip, and sharp lip with diverter.

Figure 2.- Photographs of the various inlet configurations tested.



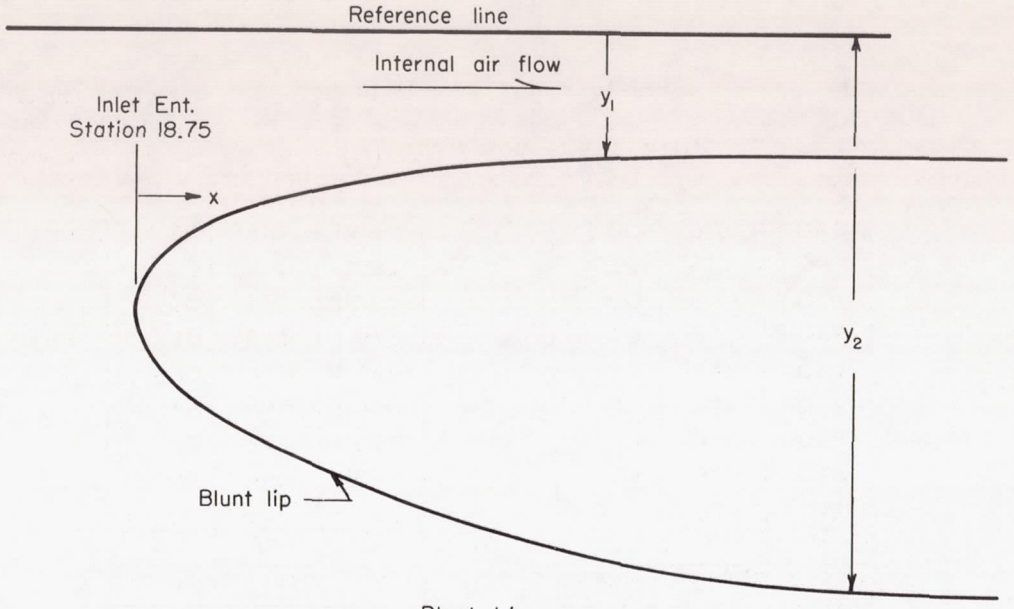
(b) Blunt lip with and without boundary-layer diverter. A-20341

Figure 2.- Continued.



(c) Thin-lip inlet with diverter, with sintered ramp, and with 0.1-inch holes in ramp. A-20342.1

Figure 2.- Concluded.



Blunt Lip

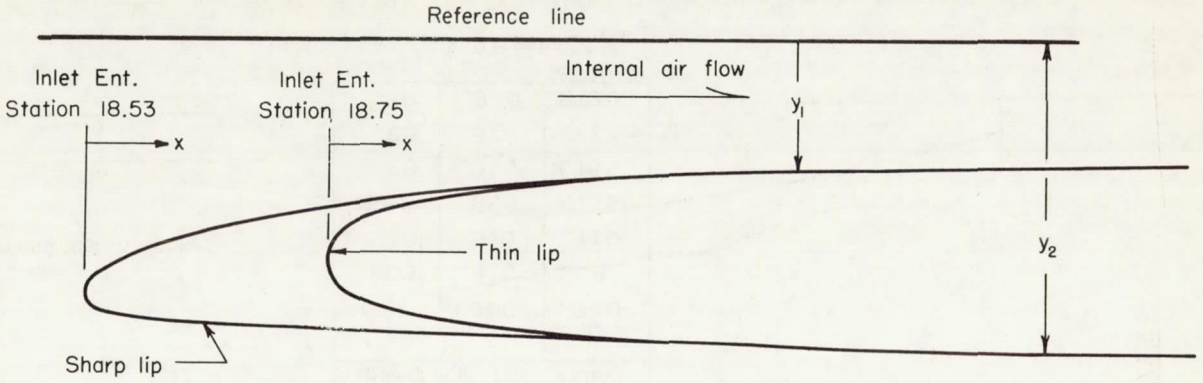
$\frac{A_{min}}{A_i} = .84$

All dimensions in inches

Leading-edge radius = .0625		
x	y_1	y_2
0	1.000	1.000
.05	.930	1.080
.10	.910	1.110
.15	.895	1.135
.20	.885	1.155
.25	.876	1.173
.30	.870	1.190

(a) Blunt lip.

Figure 3.- Sketch of the inlet lip shapes.



Thin Lip

$\frac{A_{min}}{A_i} = .96$

Leading-edge radius = .025		
x *	y_1	y_2
0	1.000	1.000
.05	.957	1.043
.10	.948	1.052
.15	.940	1.060
.20	.932	1.068
.30	.928	1.072
.50	.917	1.083
.70	.917	1.083
1.00	.910	1.090

Sharp Lip

$\frac{A_{min}}{A_i} = .90$

Leading-edge radius = .015		
x °	y_1	y_2
0	1.035	1.035
.05	.996	1.054
.10	.980	1.058
.15	.966	1.062
.20	.957	1.063
.30	.942	1.066
.50	.928	1.074
.70	.917	1.083
1.00	.915	1.086

All dimensions in inches

* x Measured from station 18.75

° x Measured from station 18.53

(b) Thin and sharp lip.

Figure 3.- Concluded.

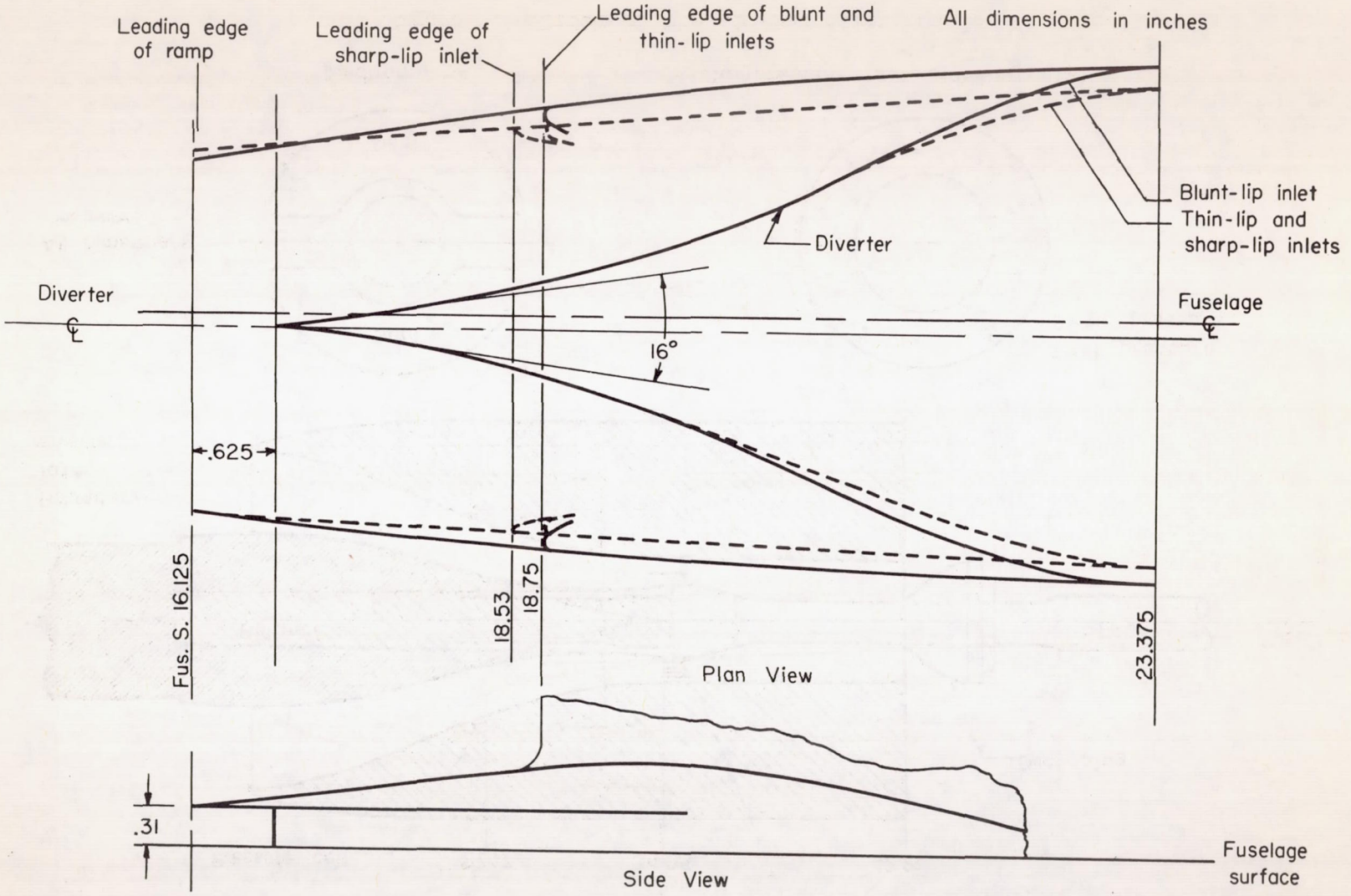


Figure 4.- A schematic drawing of the fuselage boundary-layer diverter wedges for the three inlet lip configurations.

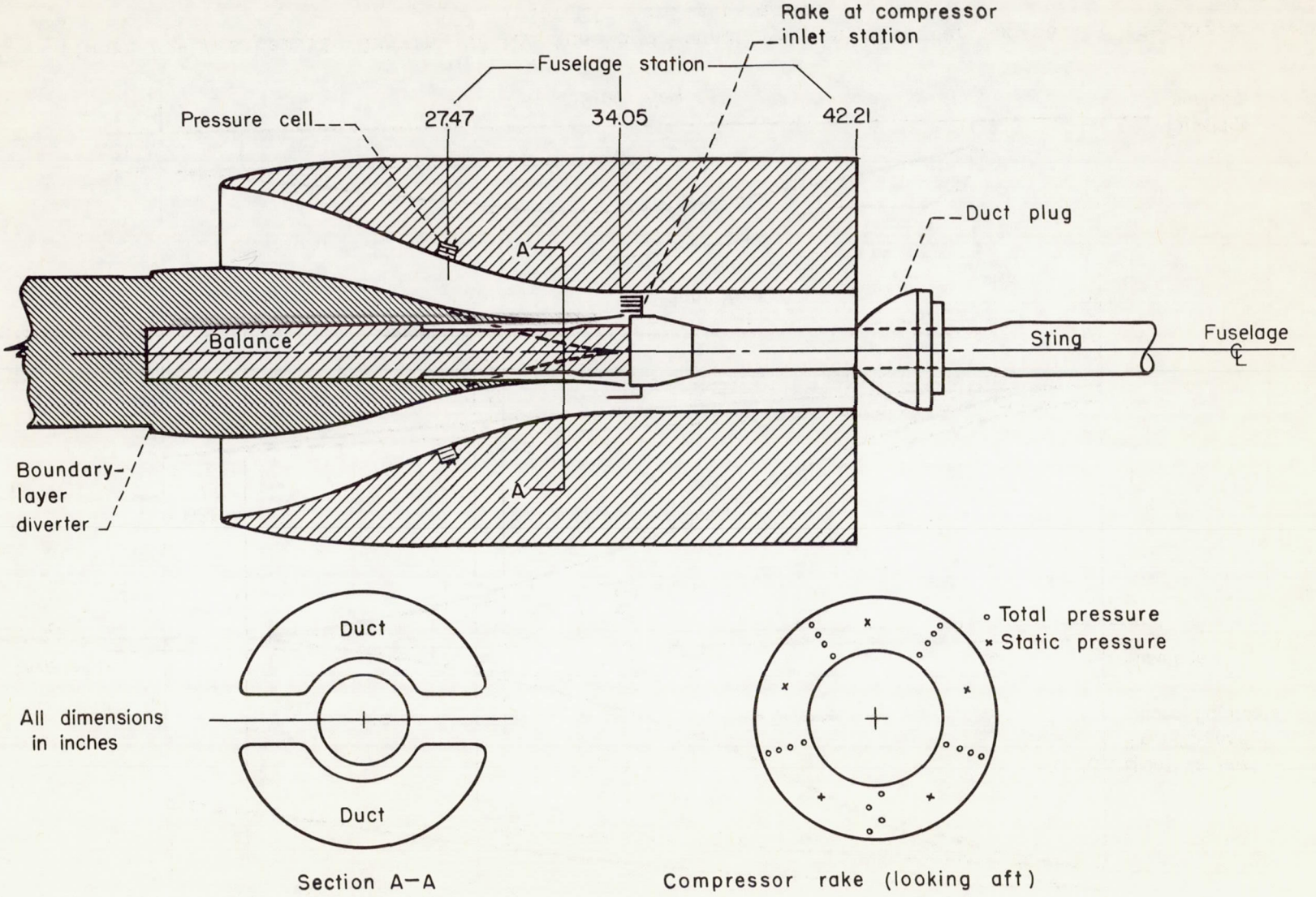


Figure 5.- Sketch of the air-induction model.

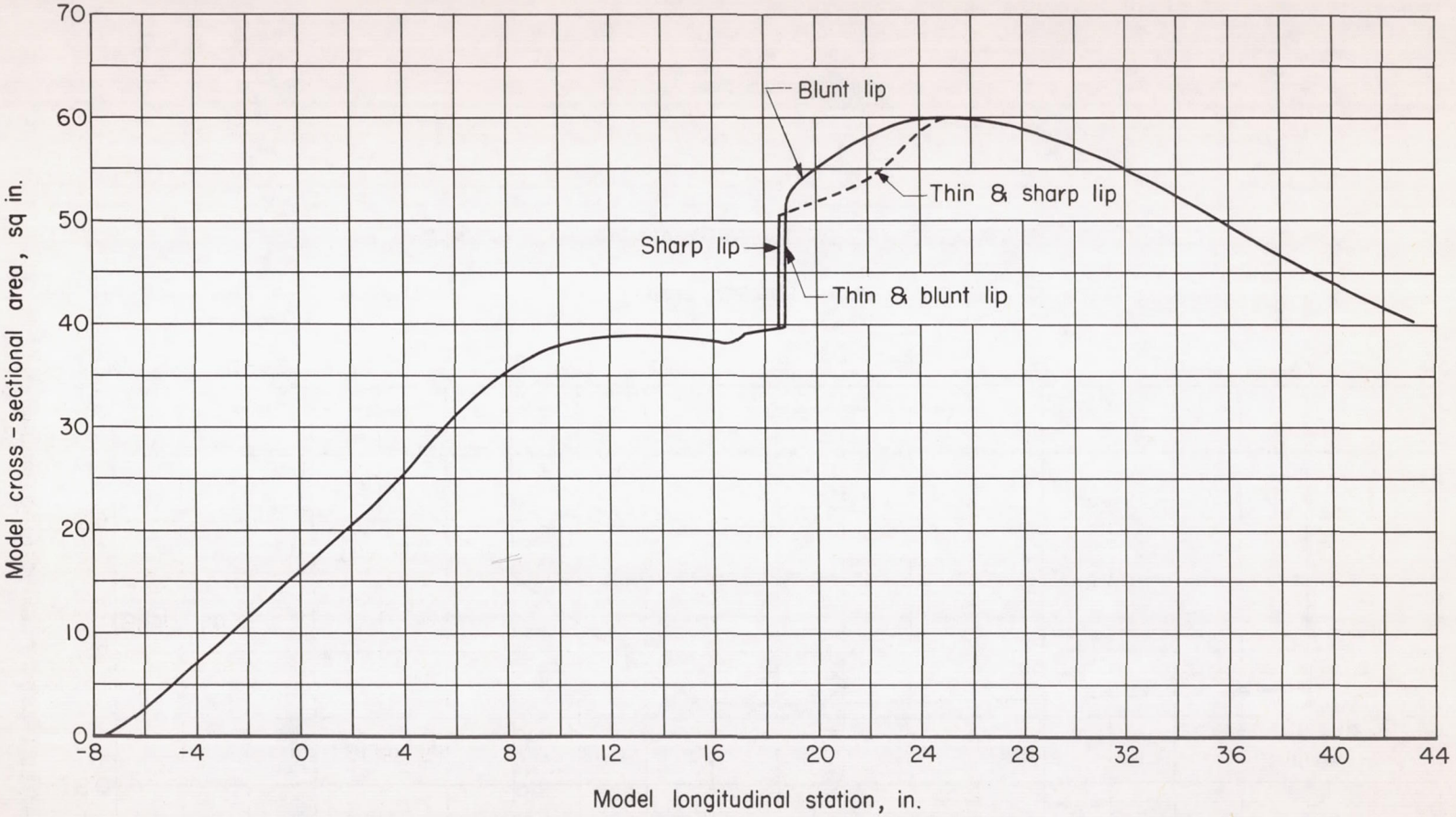


Figure 6.- Longitudinal area distribution of the air-induction model with the blunt-lip inlet, the thin-lip inlet, and the sharp-lip inlet.

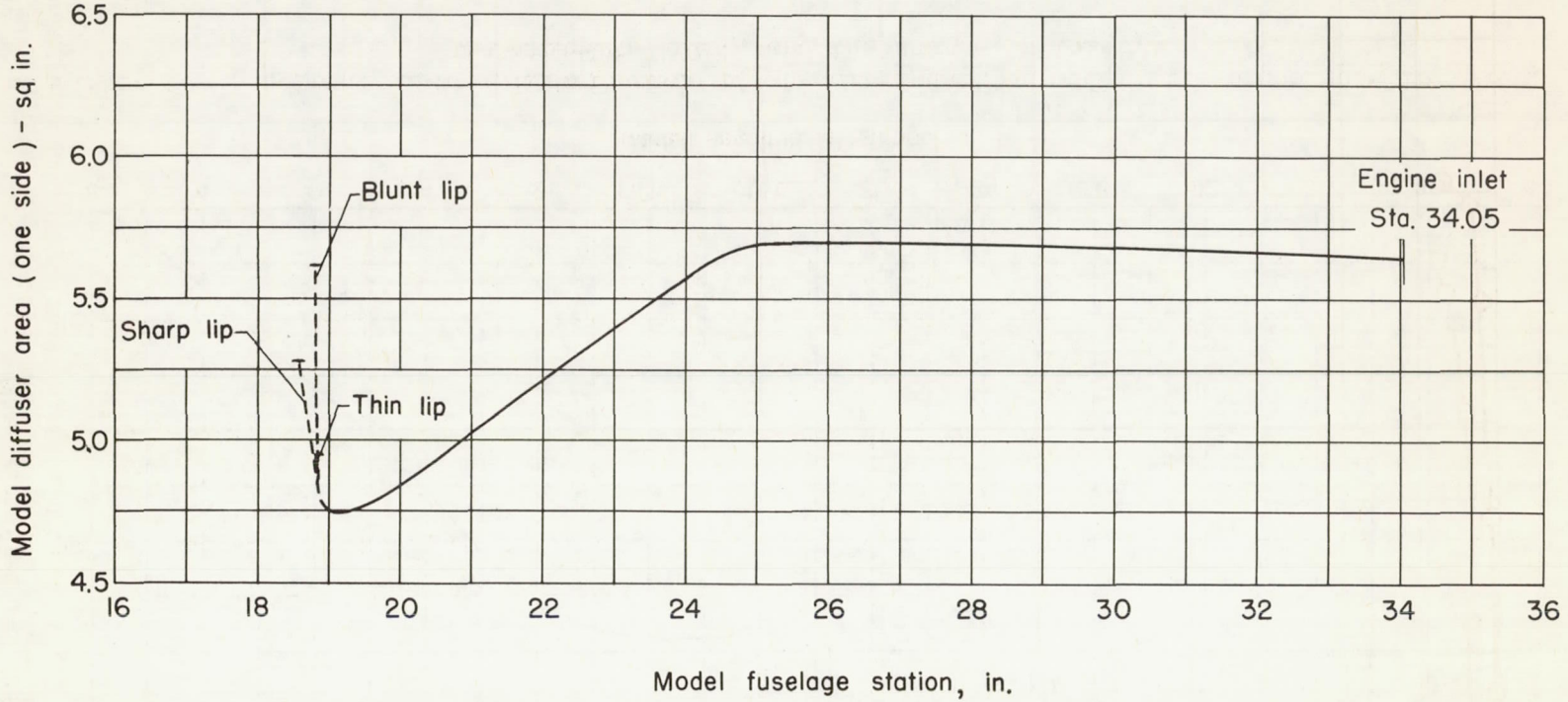
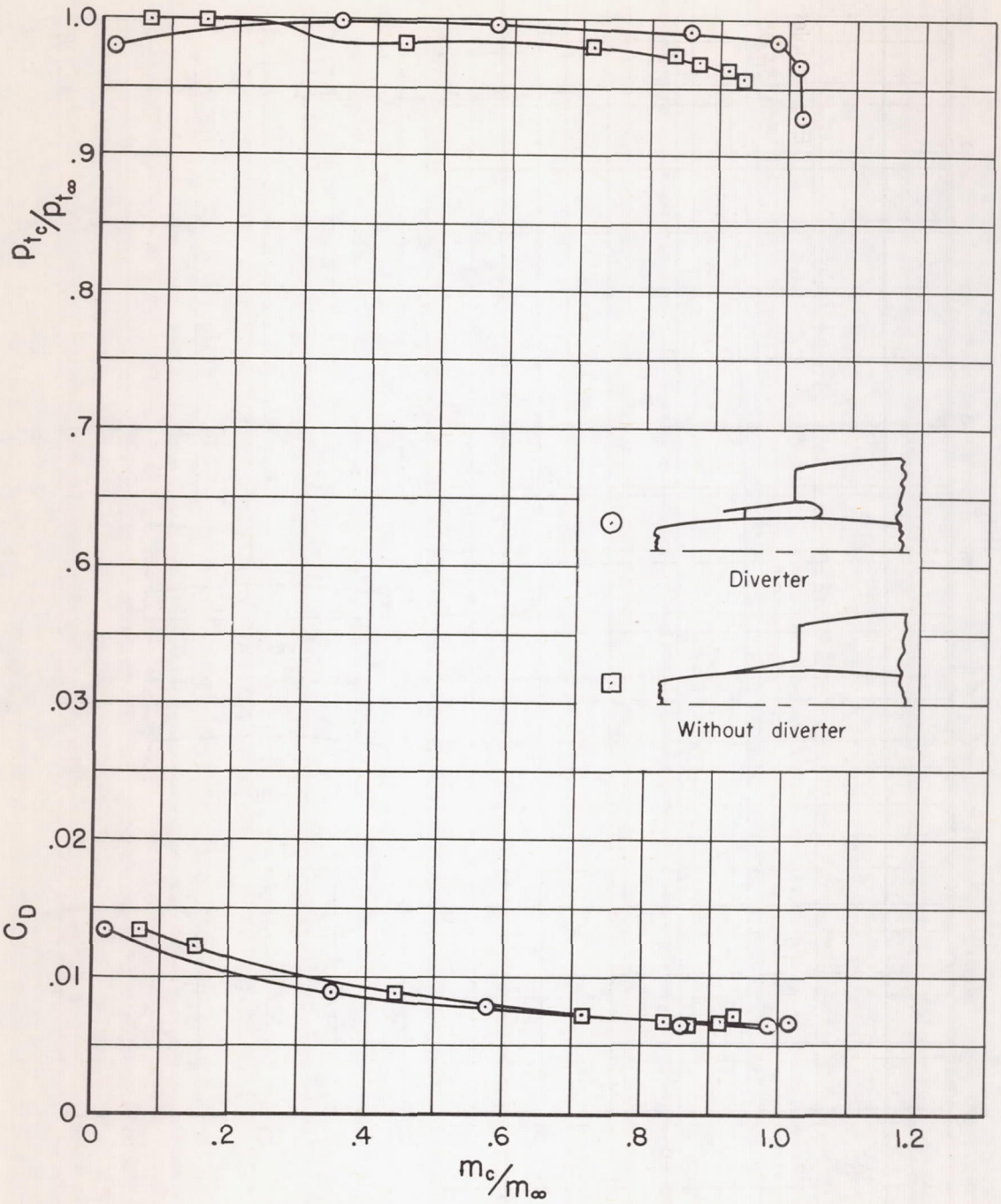
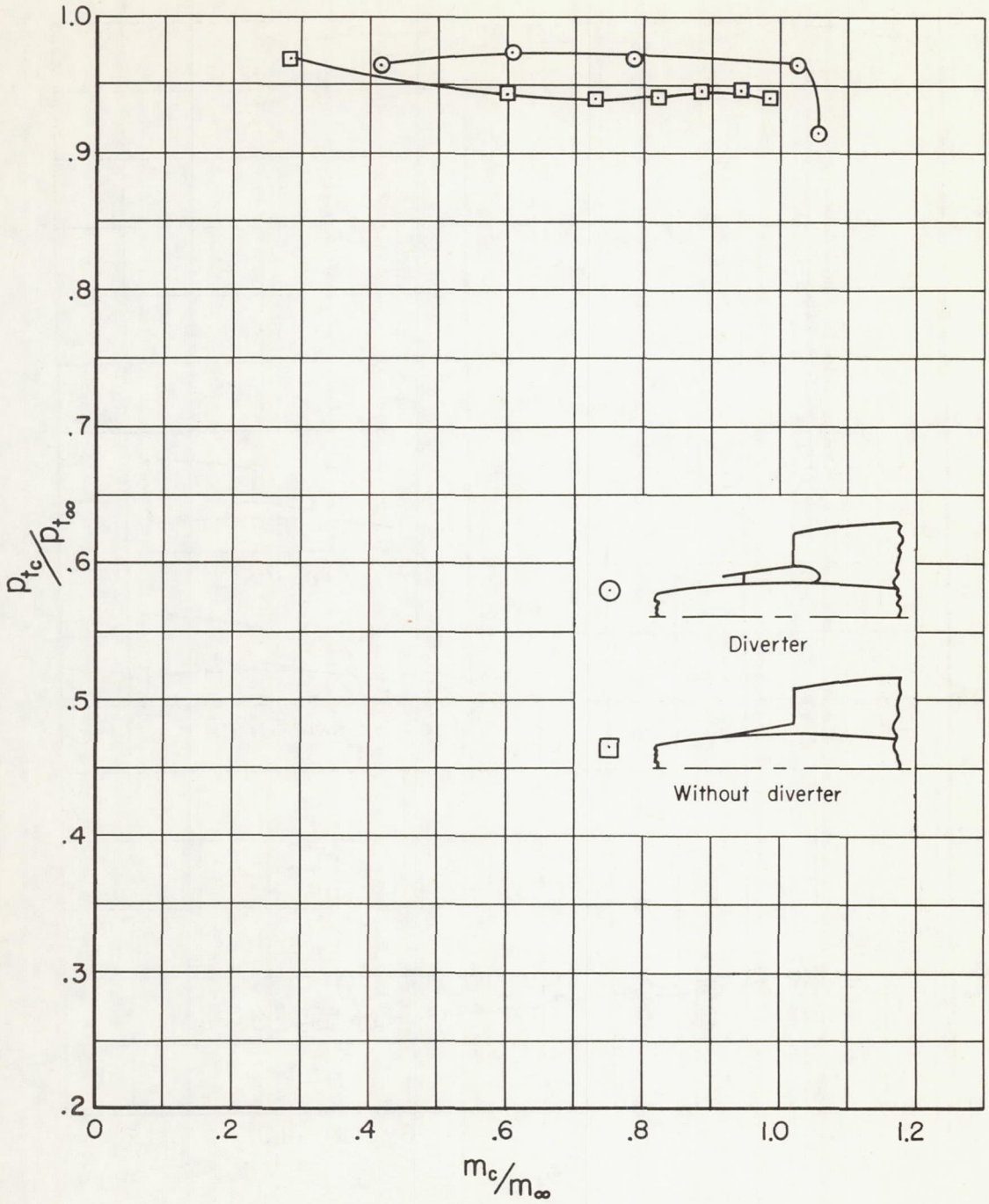


Figure 7.- Area variation in the diffuser.



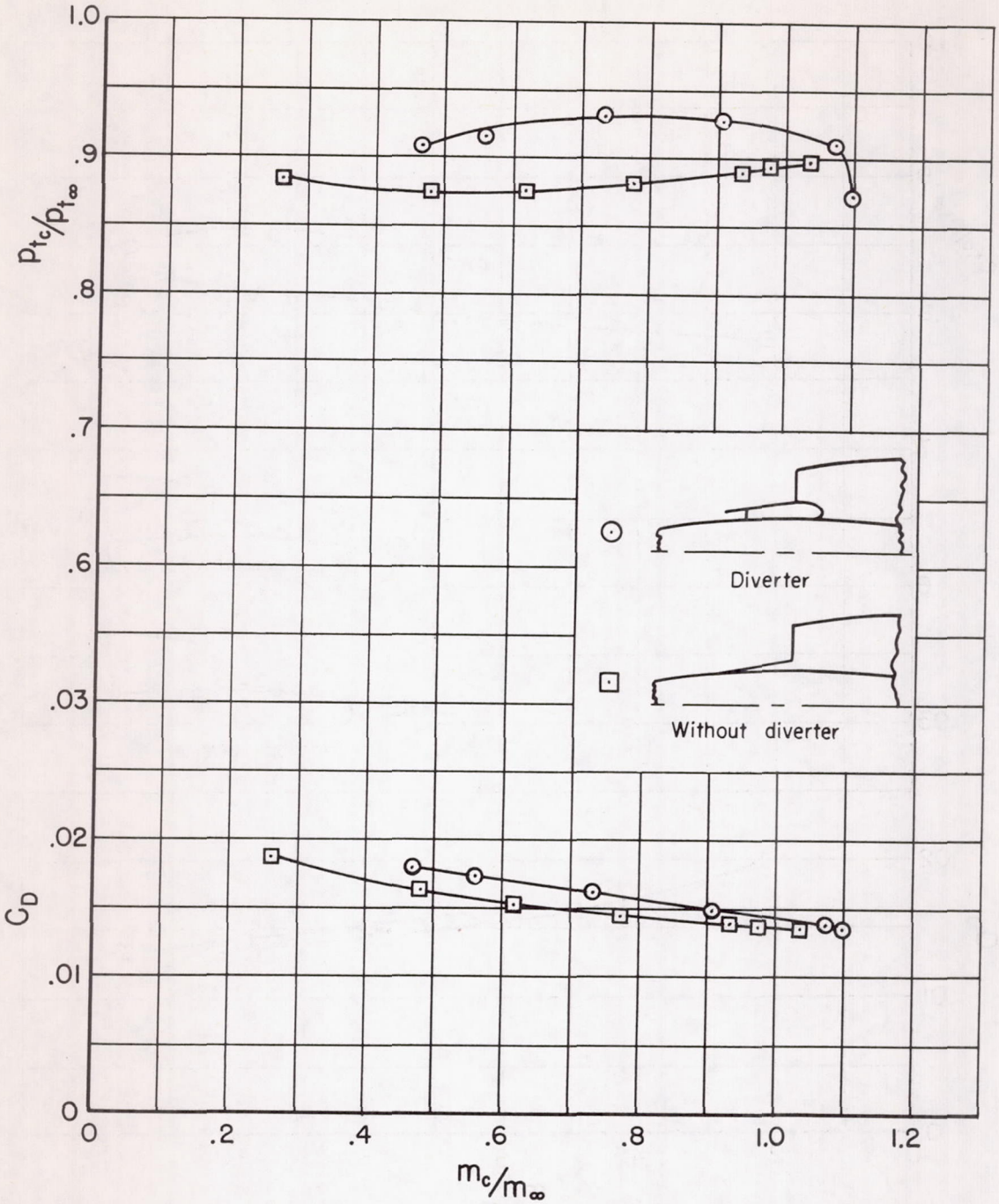
(a) $M_\infty = 0.9$

Figure 8.- The effect of the diverter-type boundary-layer removal system on the inlet performance of the blunt-lip inlet; $\alpha = 4^\circ$.



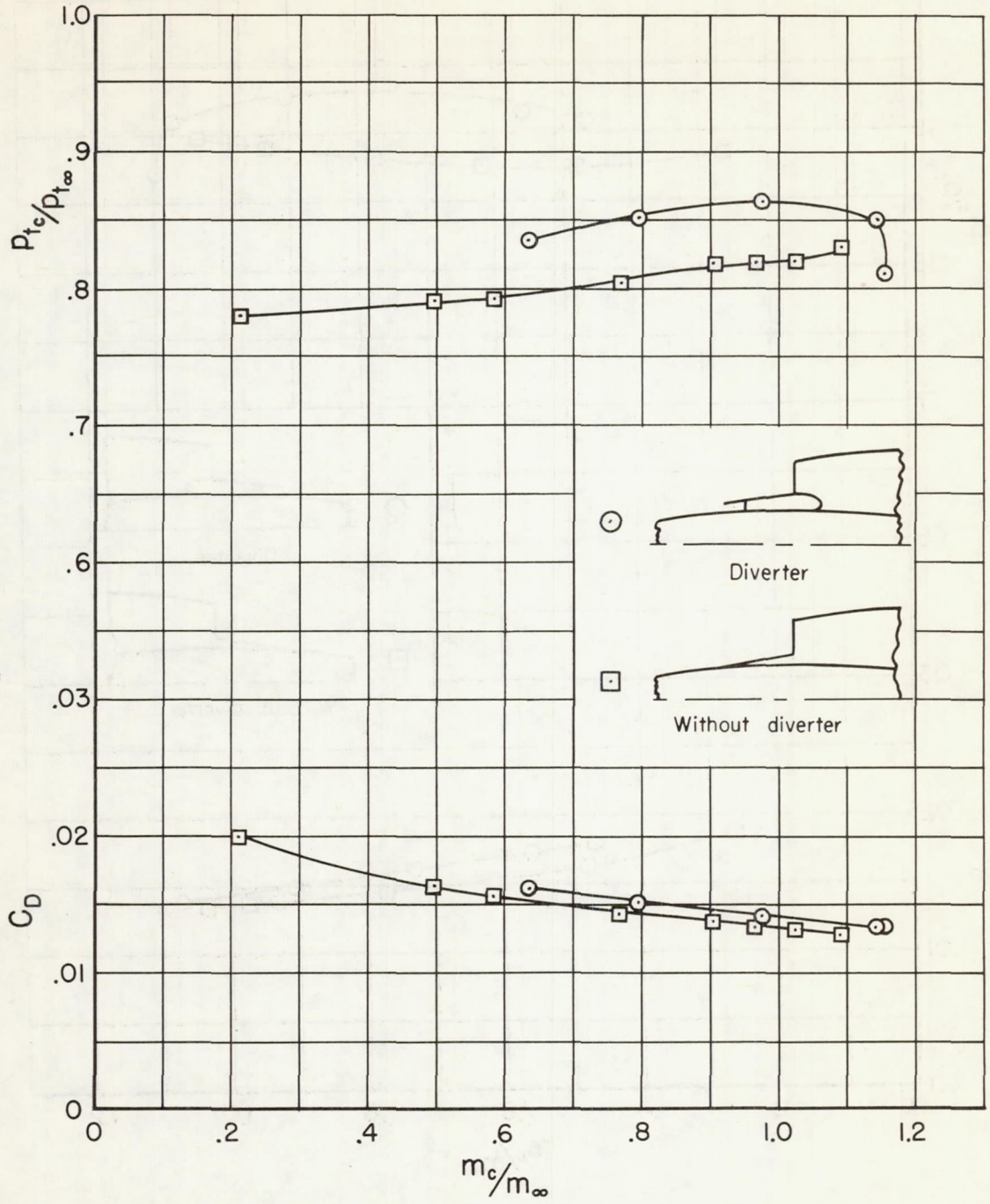
(b) $M_\infty = 1.3$

Figure 8.- Continued.



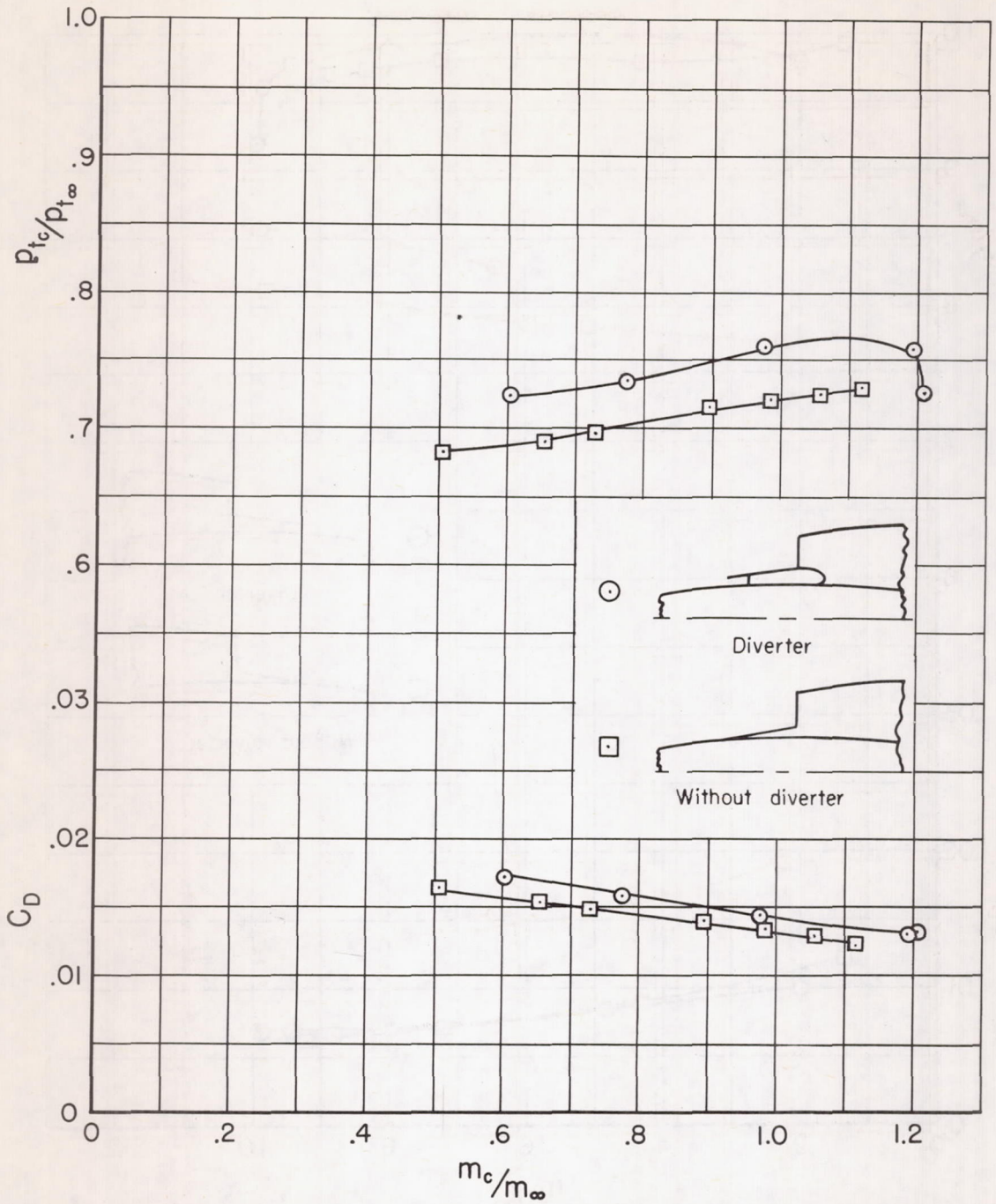
(c) $M_\infty = 1.5$

Figure 8.- Continued.



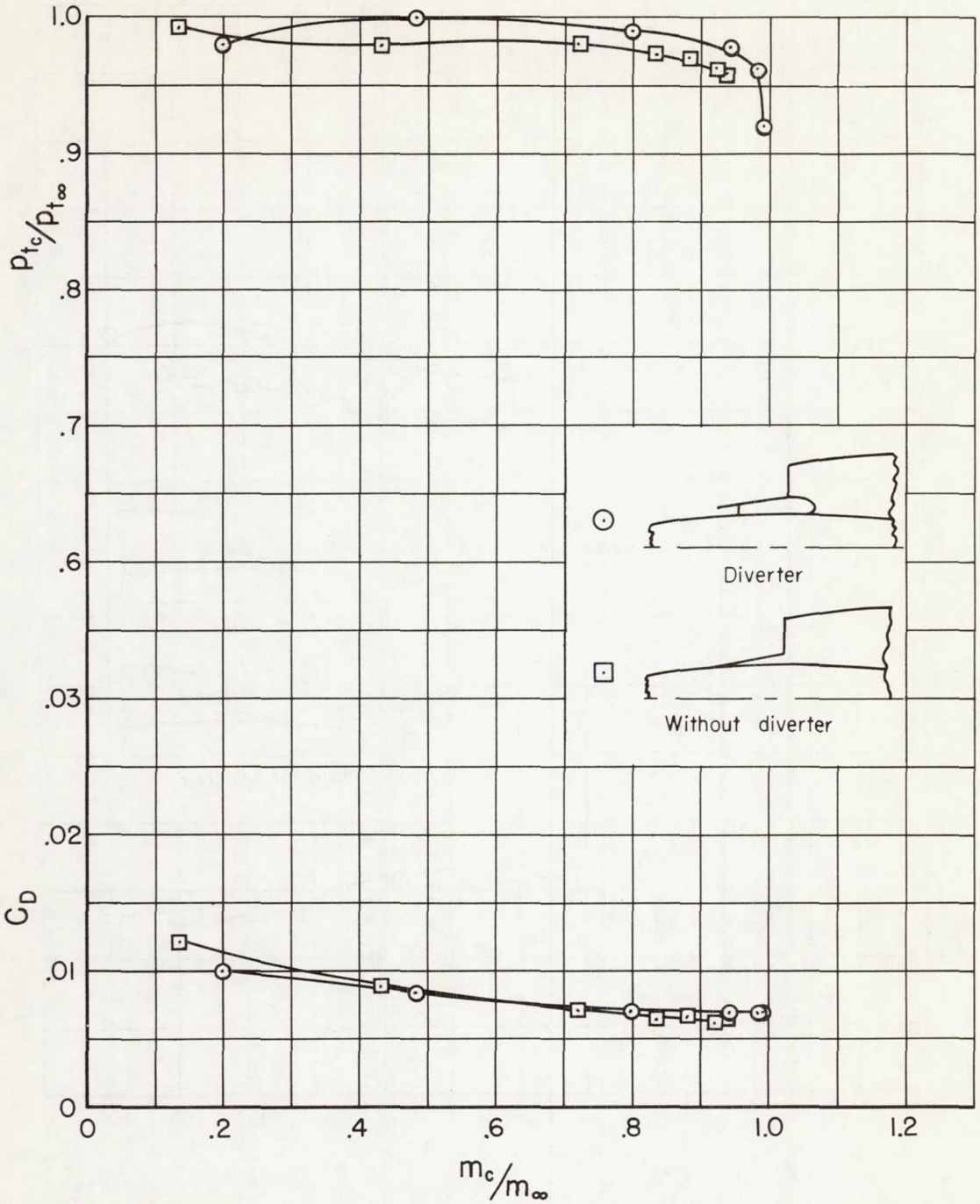
(d) $M_\infty = 1.7$

Figure 8.- Continued.



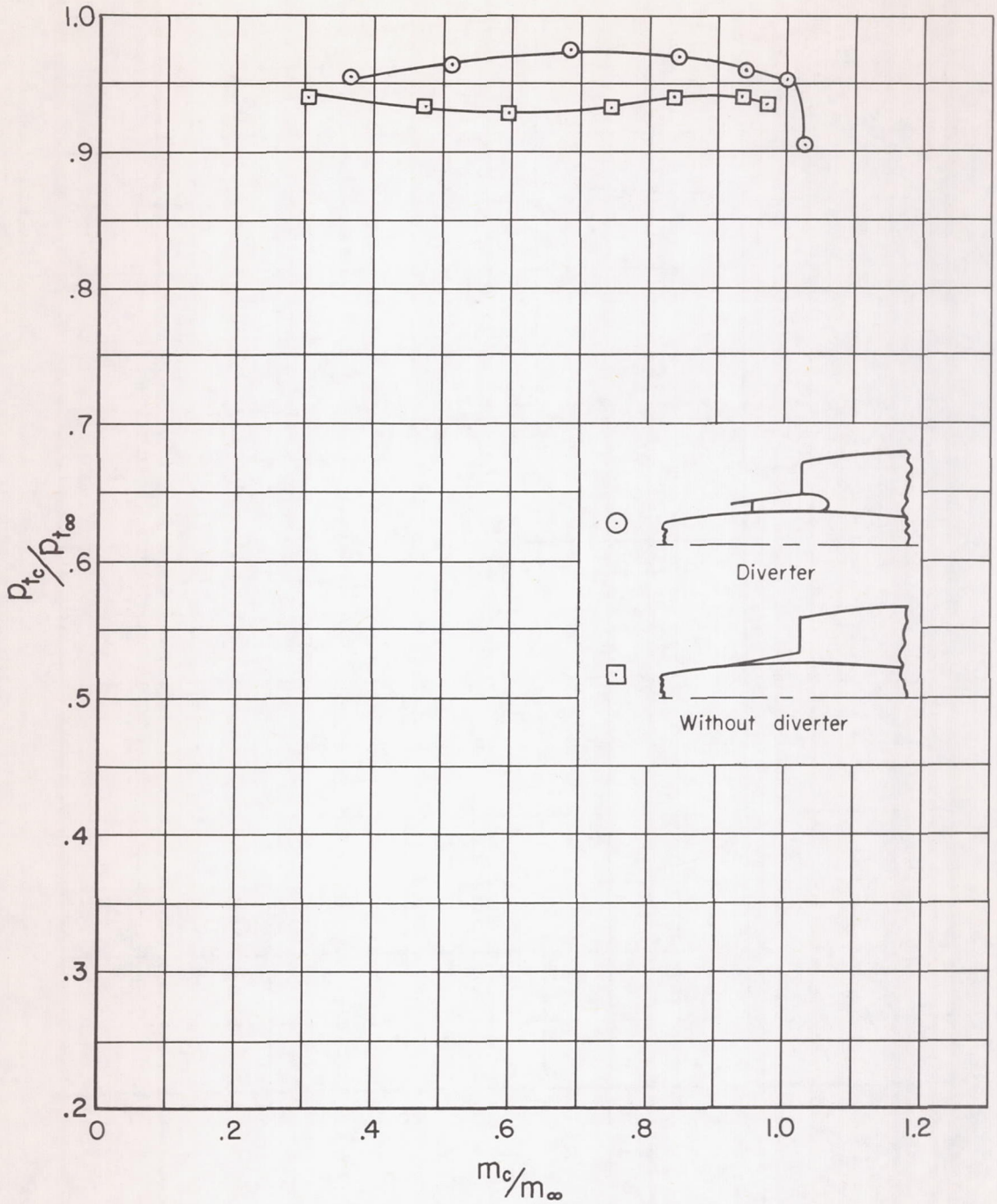
(e) $M_\infty = 1.9$

Figure 8.- Concluded.



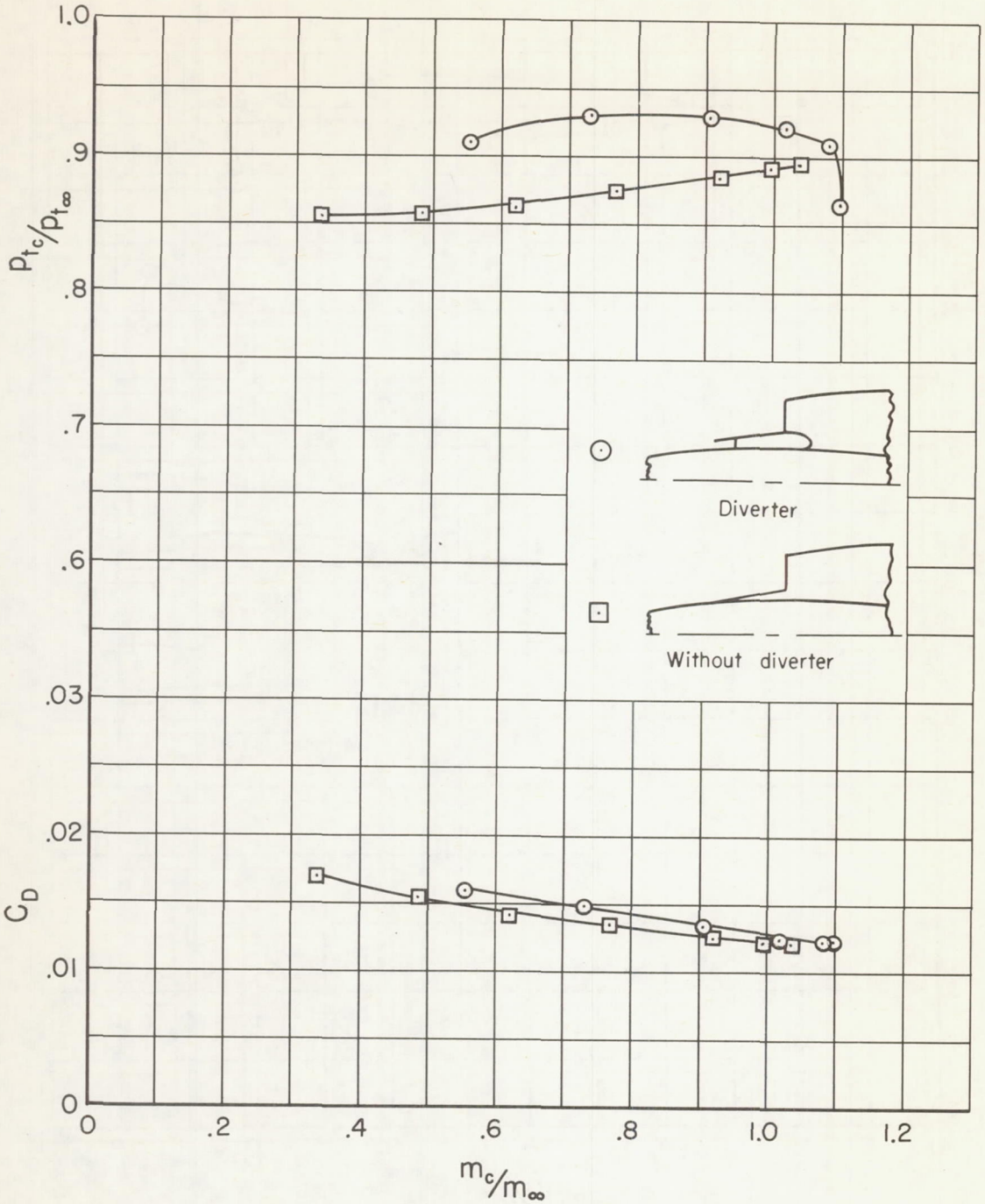
(a) $M_\infty = 0.9$

Figure 9.- The effect of the diverter-type boundary-layer control system on the inlet performance of the thin-lip inlet; $\alpha = 4^\circ$.



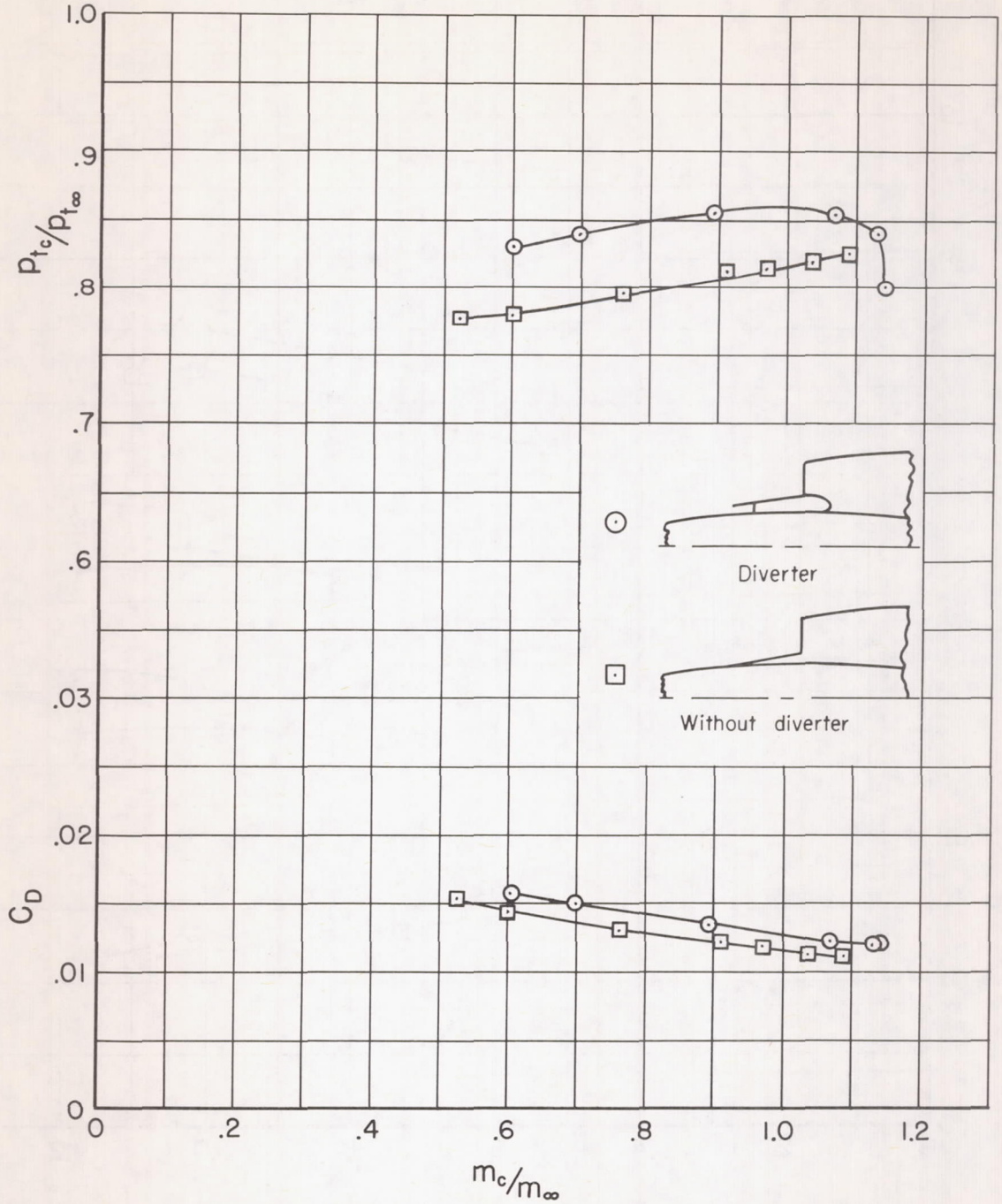
(b) $M_\infty = 1.3$

Figure 9.- Continued.



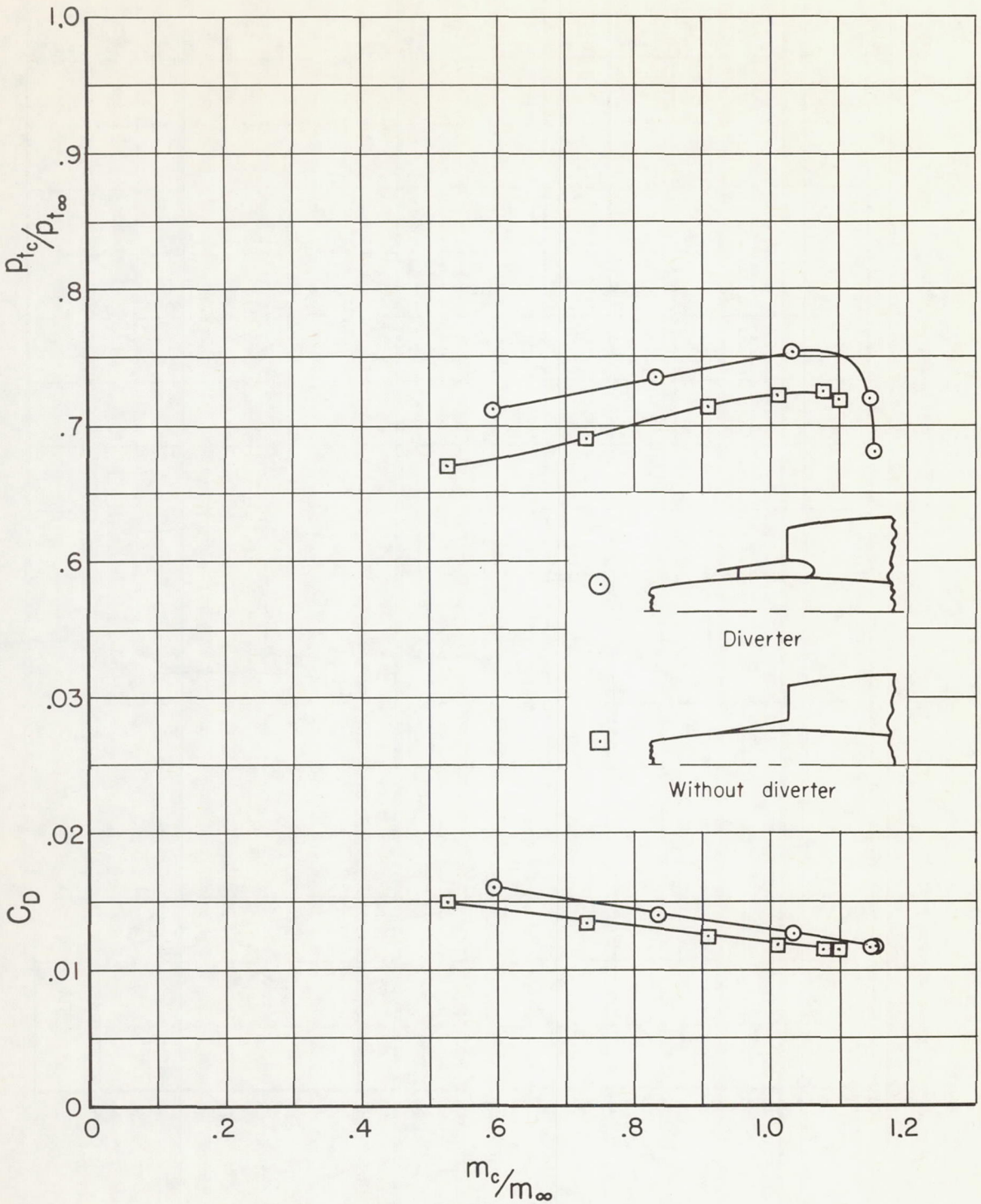
(c) $M_\infty = 1.5$

Figure 9.- Continued.



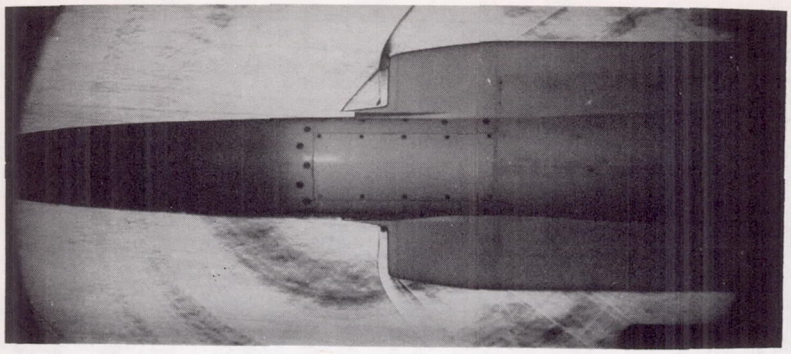
(d) $M_\infty = 1.7$

Figure 9.- Continued.

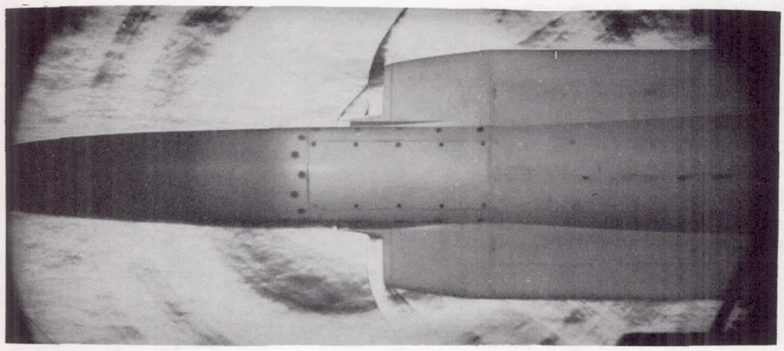


(e) $M_\infty = 1.9$

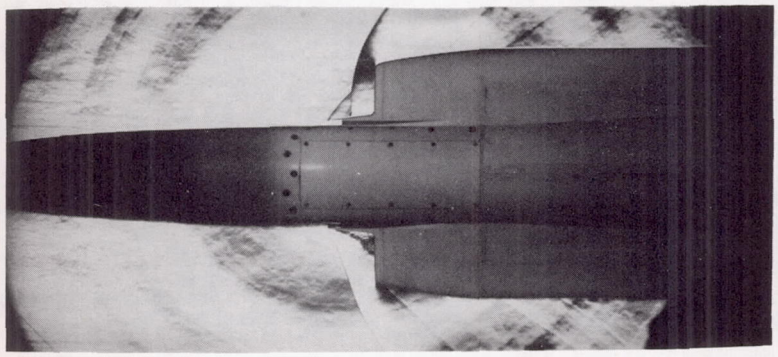
Figure 9.- Concluded.



m_c/m_∞ = max



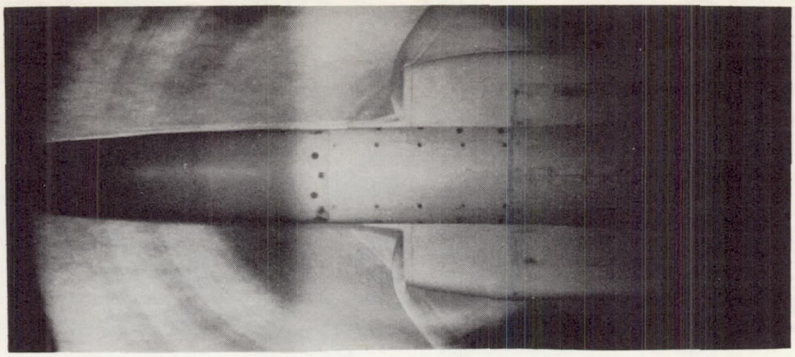
$m_c/m_\infty \approx 0.9$



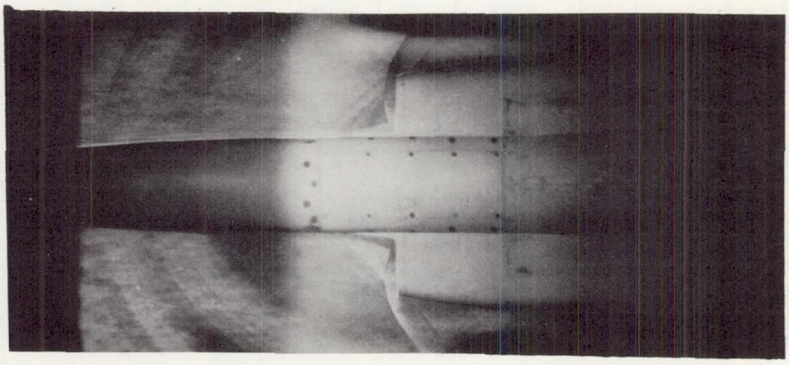
$m_c/m_\infty \approx 0.6$ A-19526

(a) With diverter.

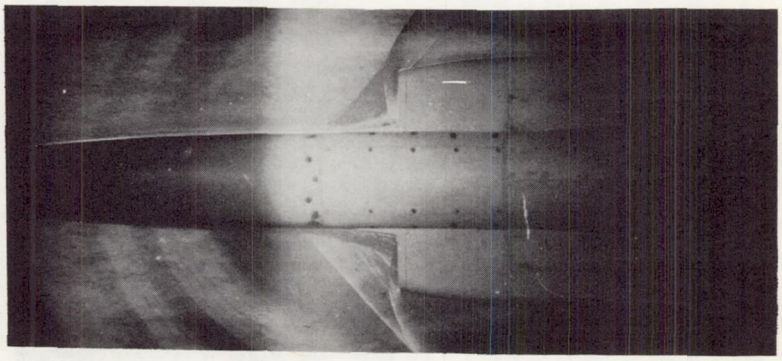
Figure 10.- Schlieren photographs of the air-induction model with the blunt-lip inlet with and without diverter; $M_\infty = 1.5$, $\alpha = 4^c$.



m_c/m_∞ = max



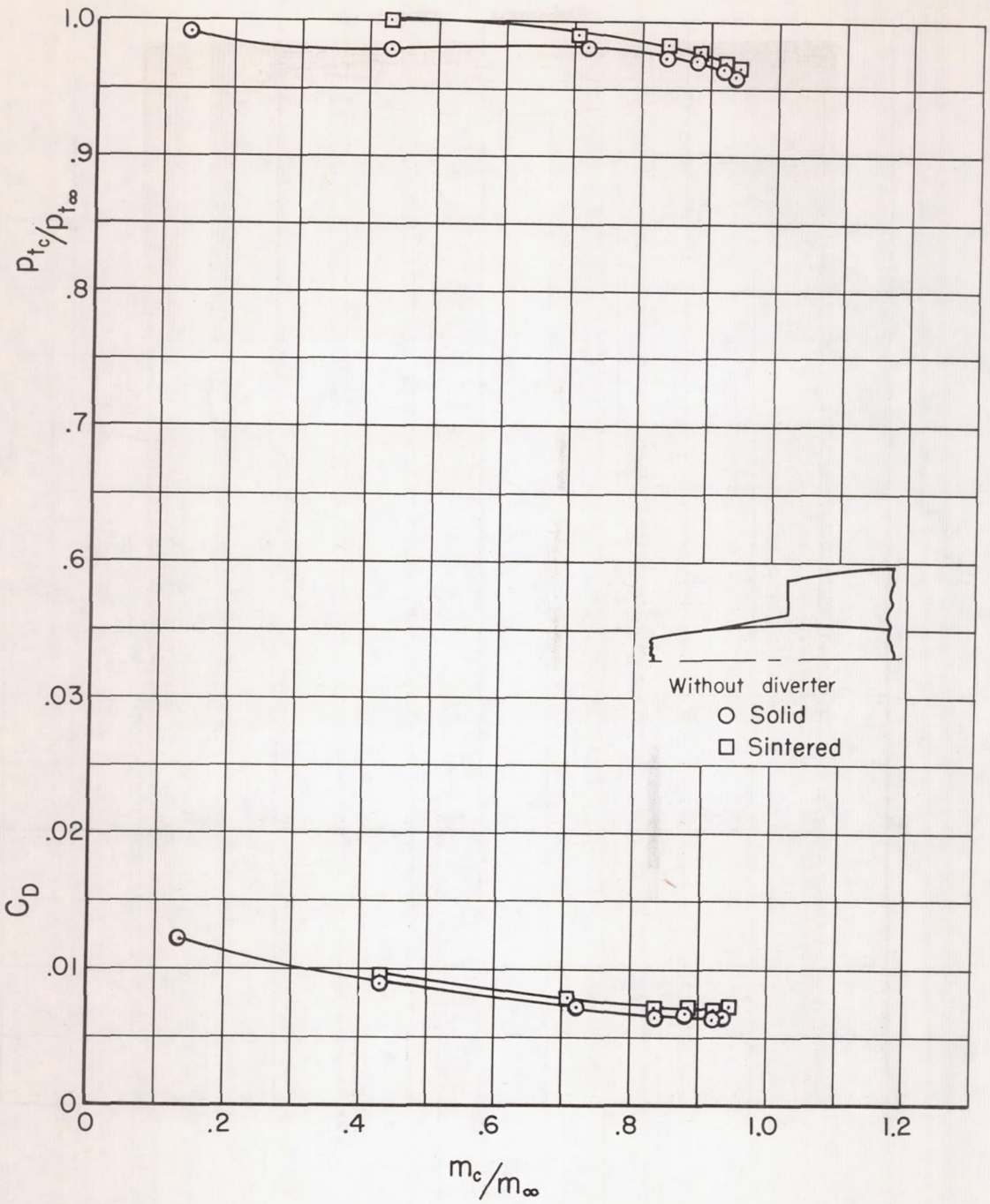
$m_c/m_\infty \approx 0.9$



$m_c/m_\infty \approx 0.6$ A-20785

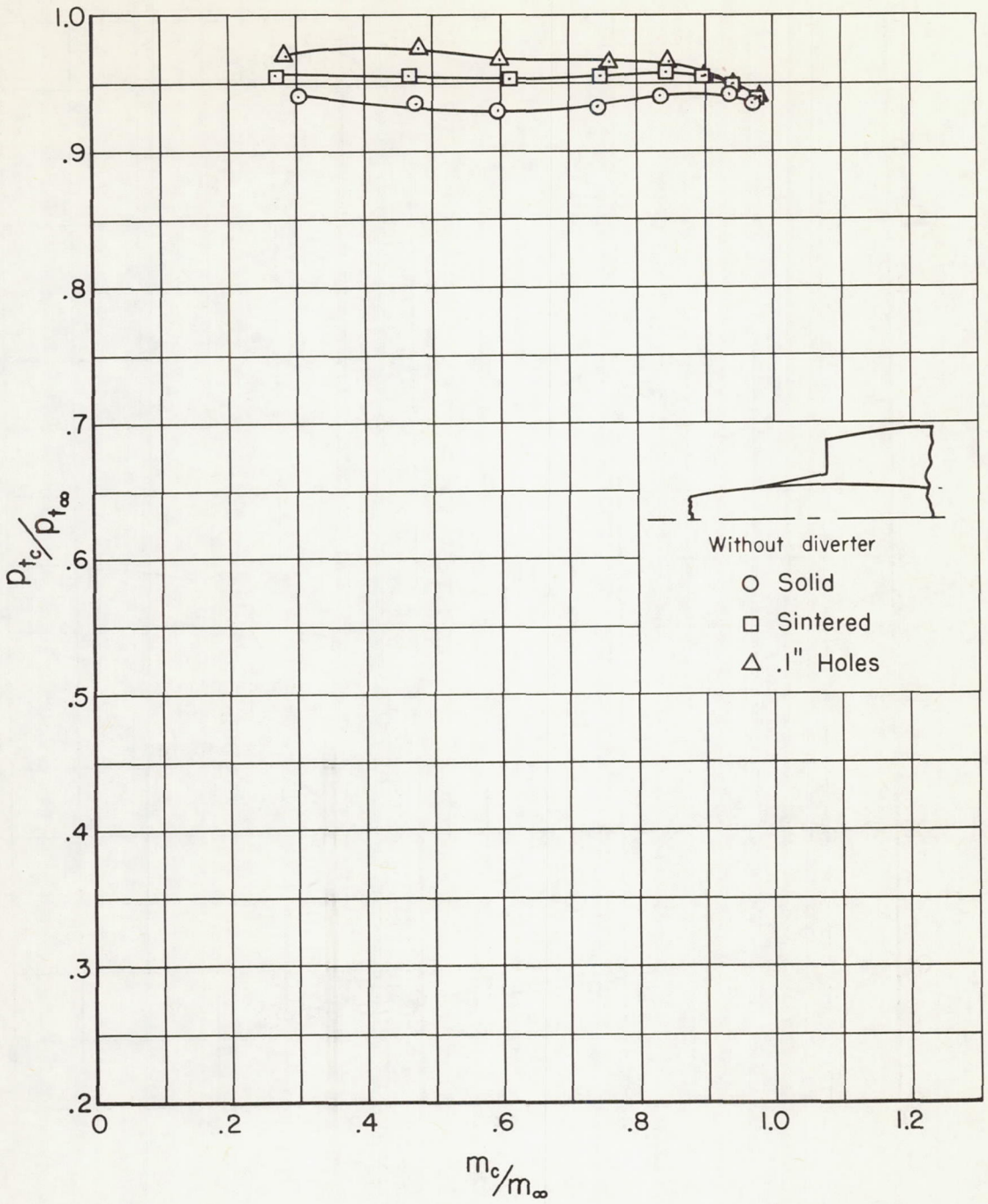
(b) Without diverter.

Figure 10.- Concluded.



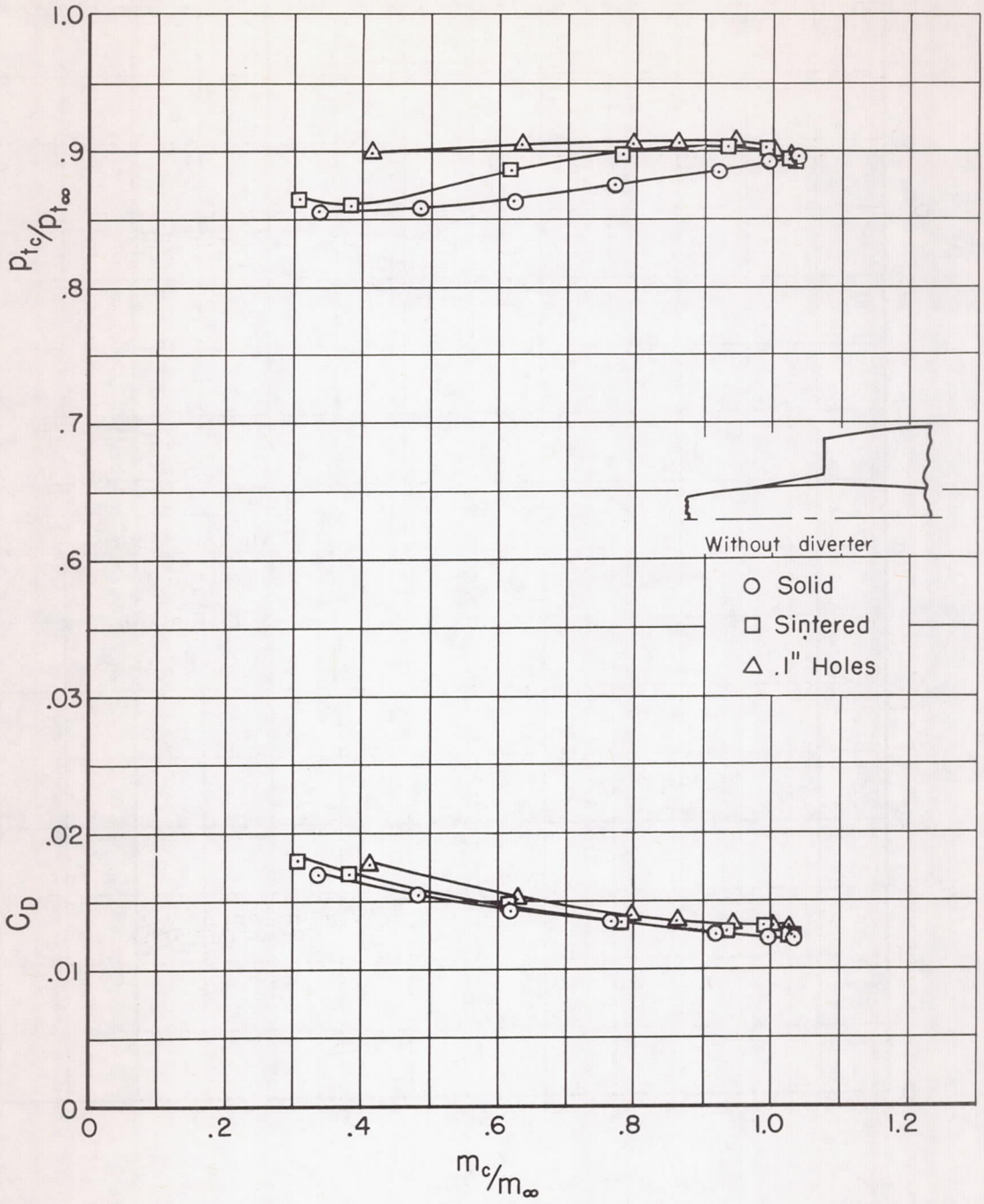
(a) $M_\infty = 0.9$

Figure 11.- The effect of ramp porosity on the total-pressure-recovery ratio and drag coefficient of the thin-lip inlet; $\alpha = 4^\circ$, ramp angle = 7°.



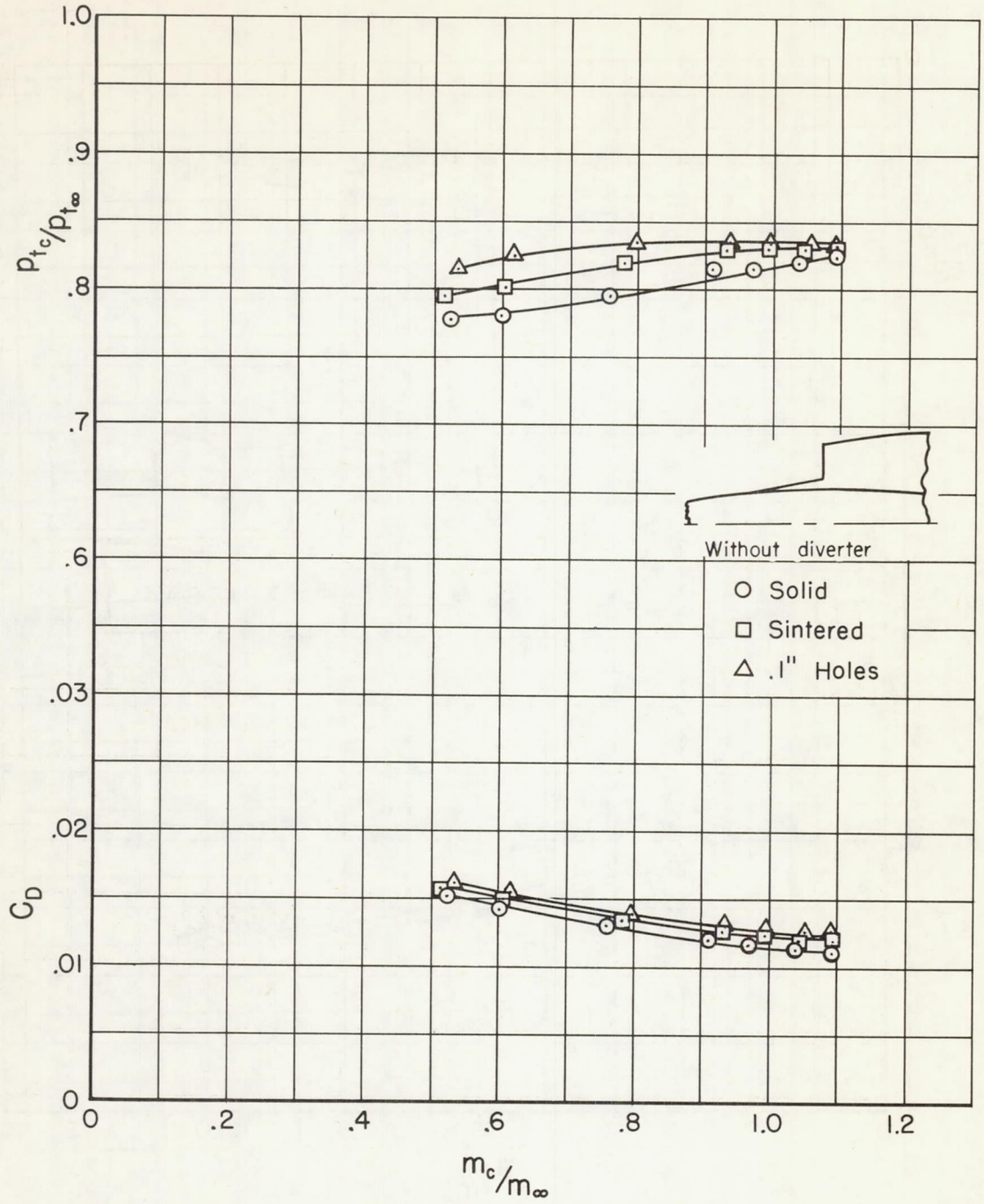
(b) $M_\infty = 1.3$

Figure 11.- Continued.



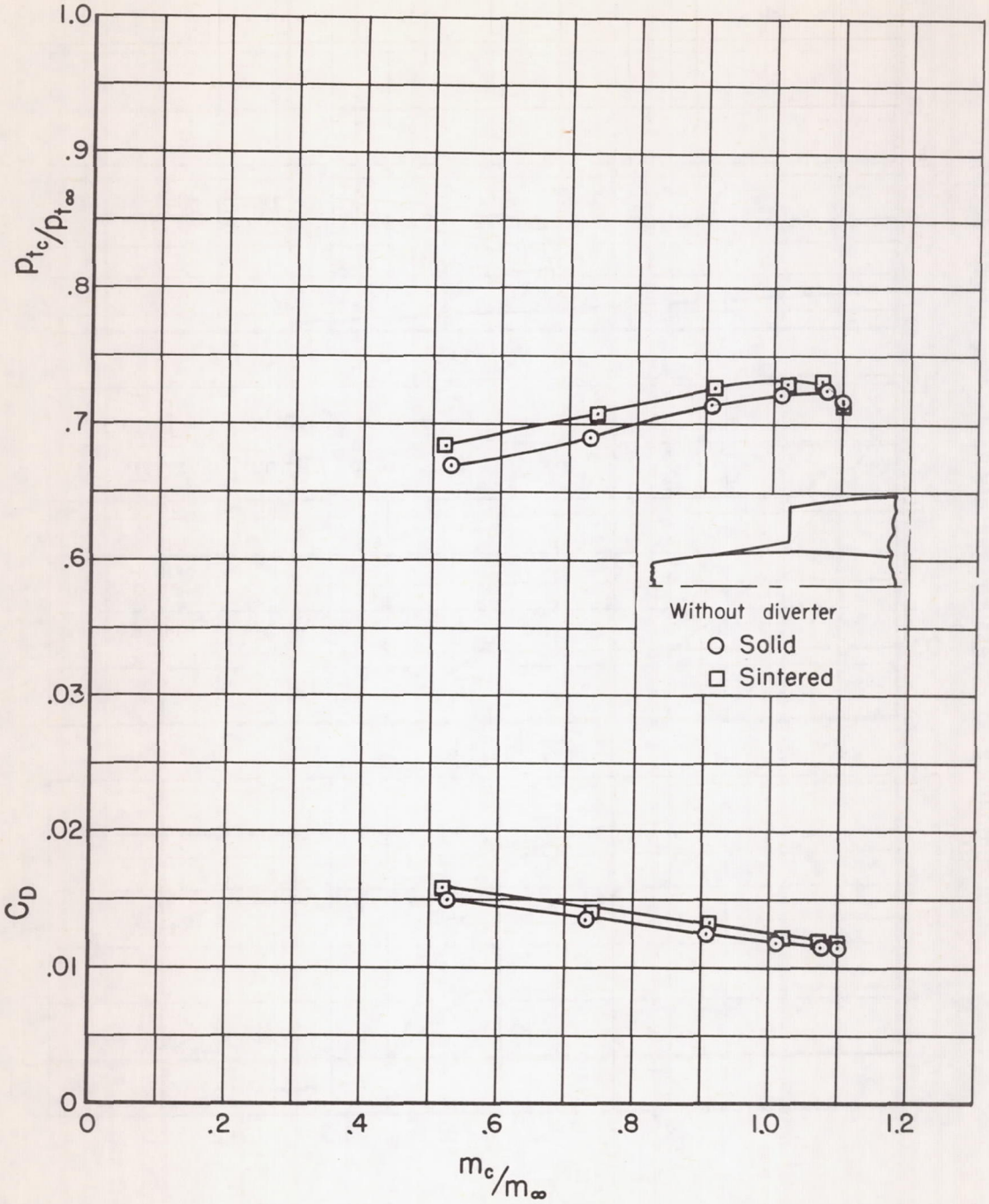
(c) $M_\infty = 1.5$

Figure 11.- Continued.



(d) $M_\infty = 1.7$

Figure 11.- Continued.



(e) $M_\infty = 1.9$

Figure 11.- Concluded.

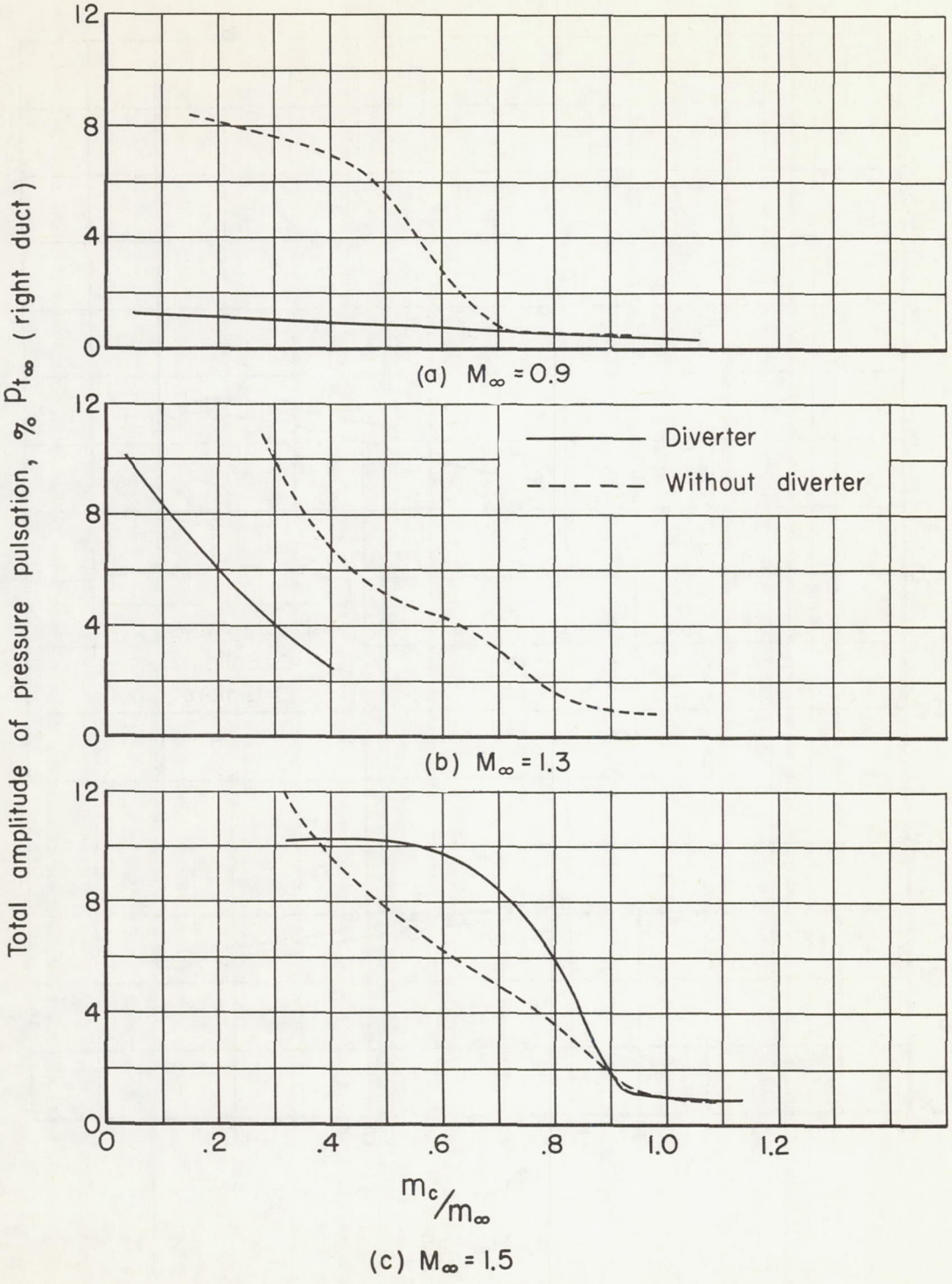


Figure 12.- Total amplitude of the pressure oscillations for the blunt-lip inlet with and without diverter; $\alpha = 4^\circ$.

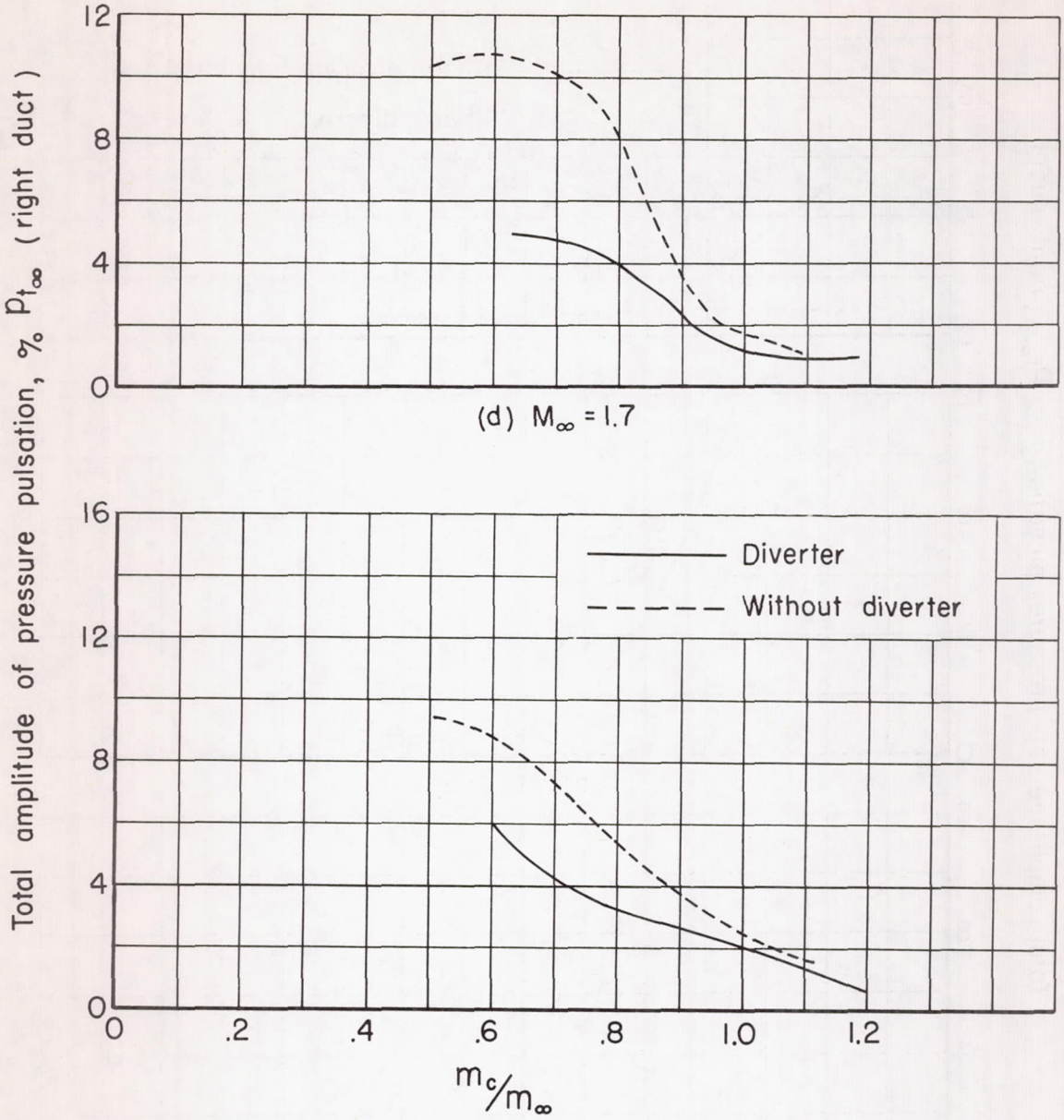


Figure 12.- Concluded.

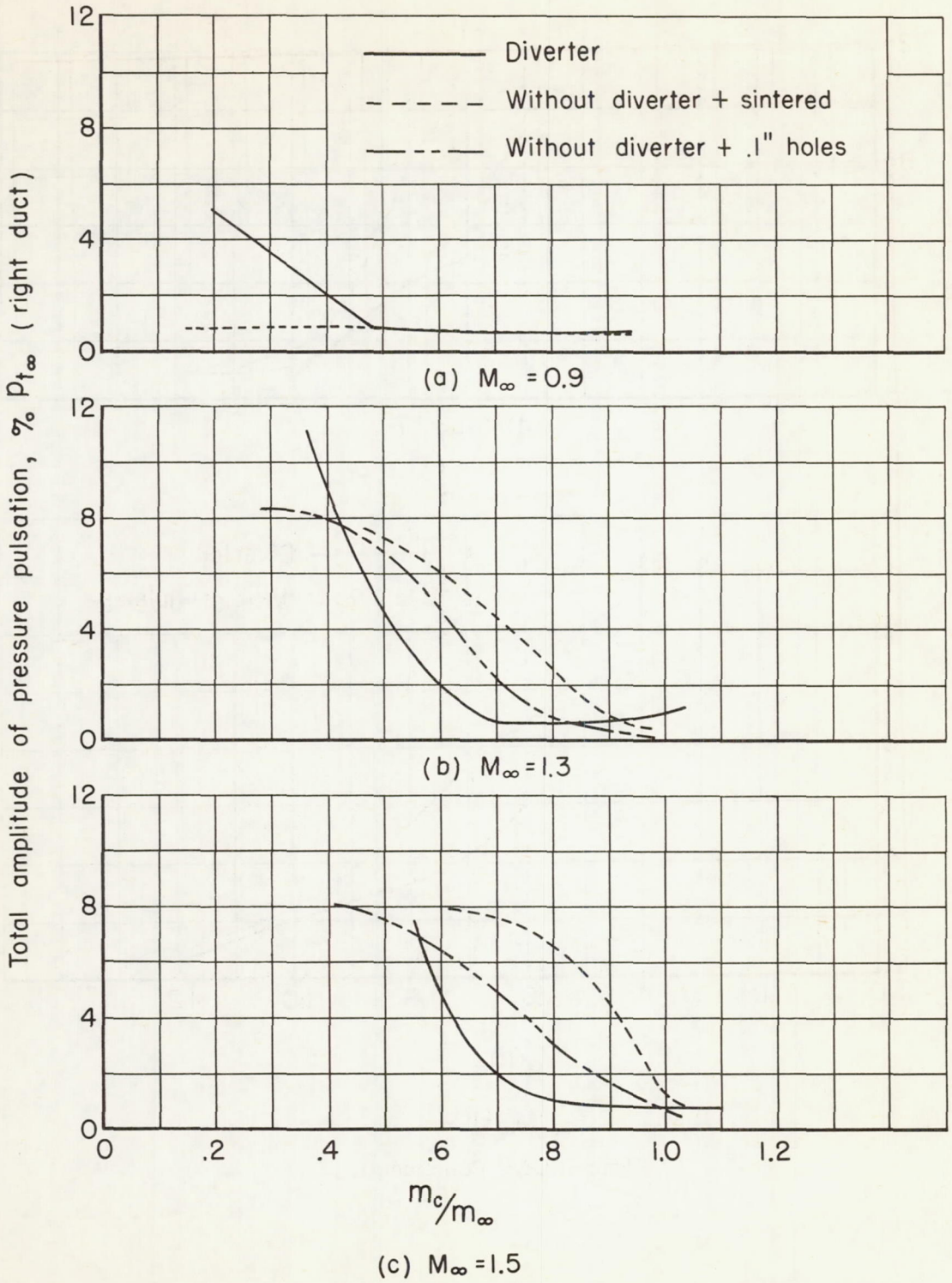


Figure 13.- Total amplitude of the pressure oscillations for the thin-lip inlet configurations; $\alpha = 4^\circ$.

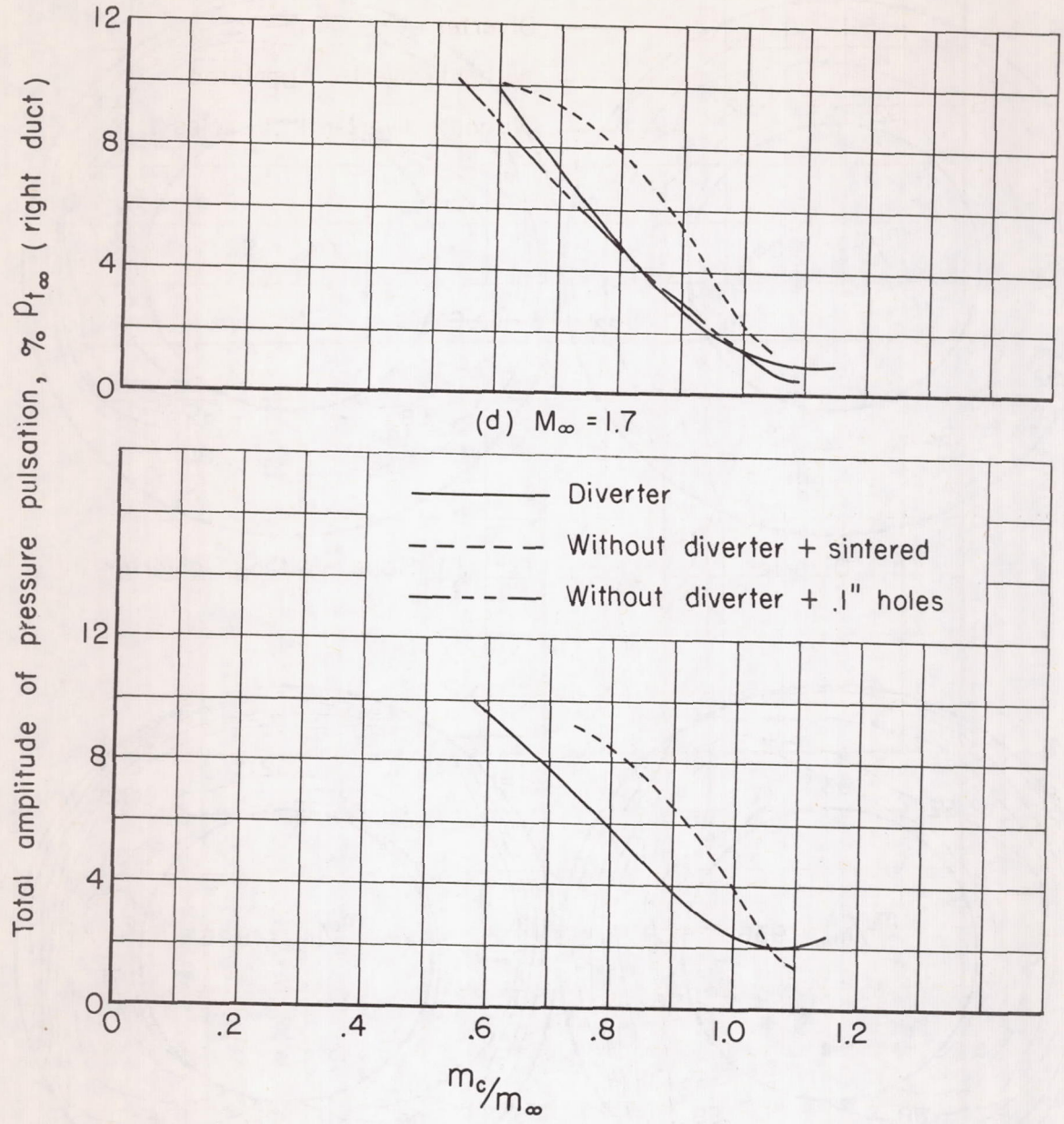


Figure 13.- Concluded.

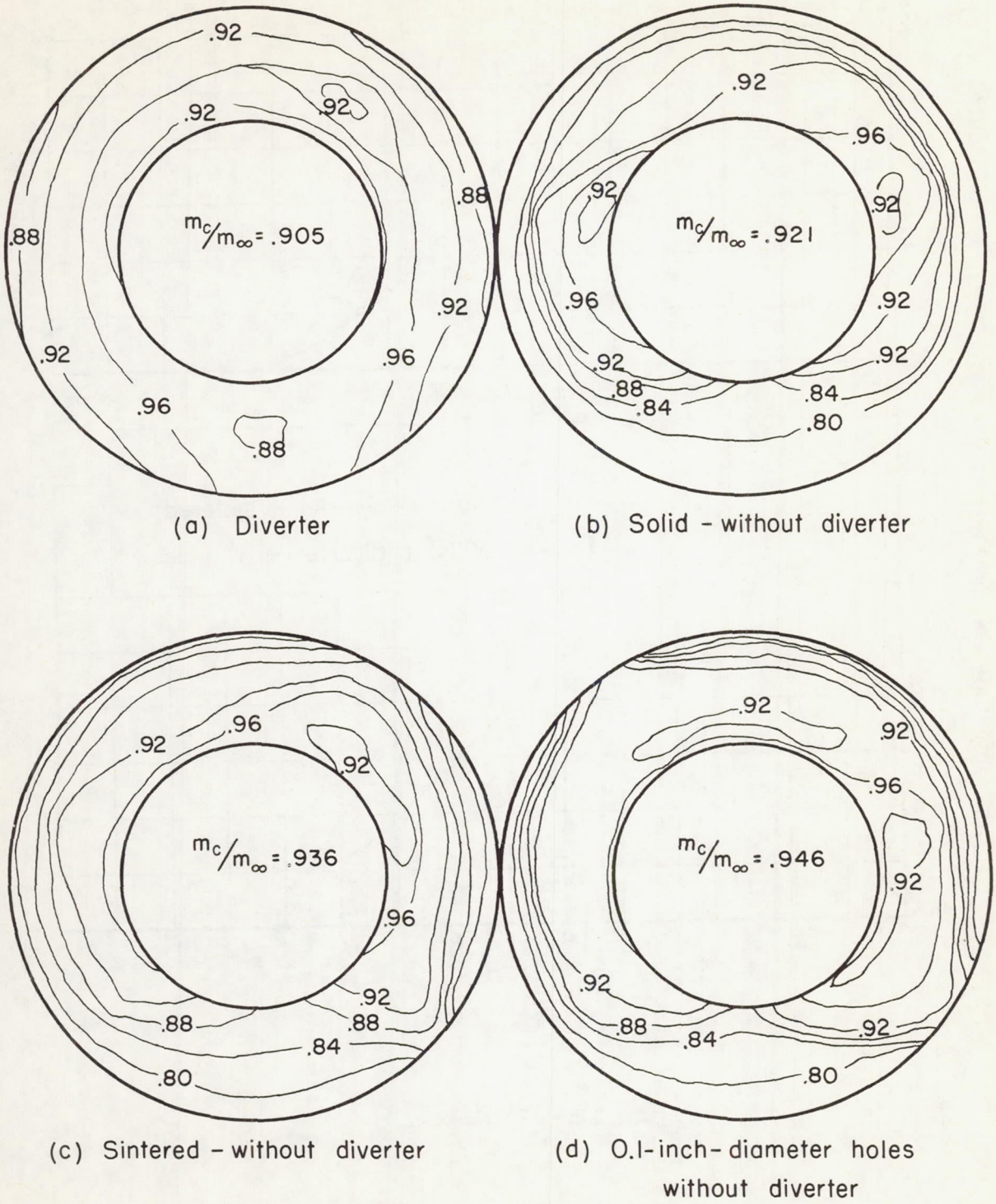
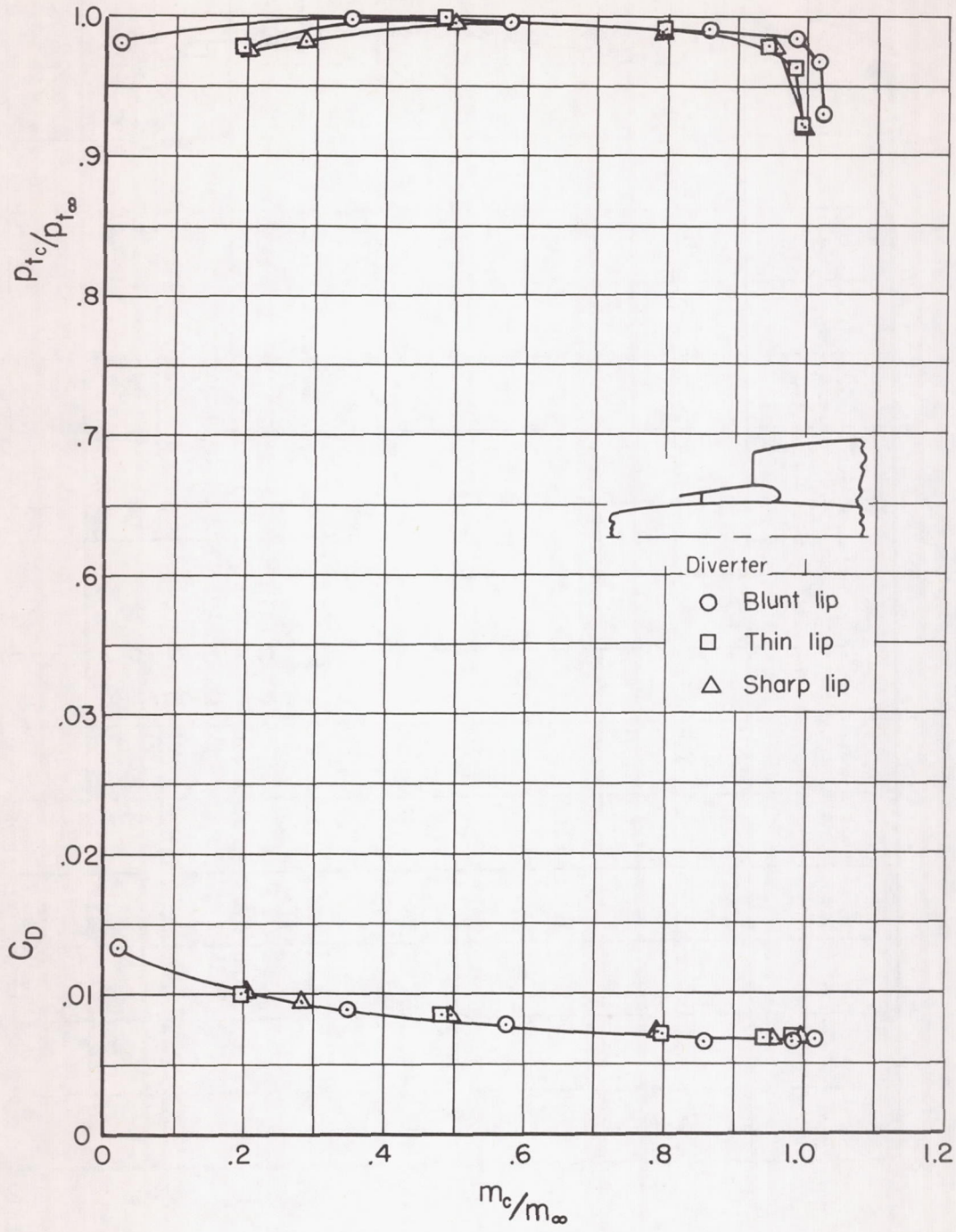
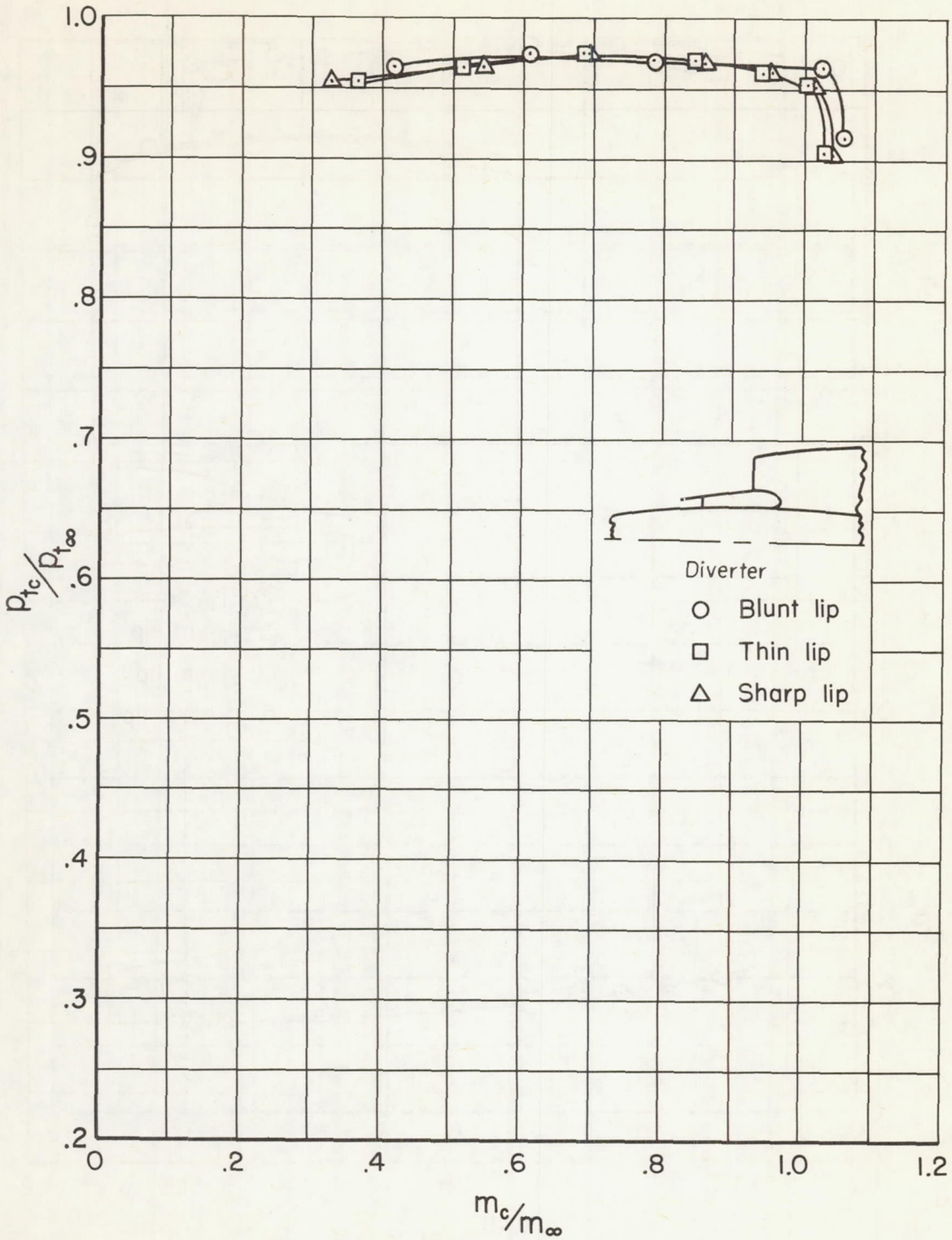


Figure 14.- Typical total-pressure-recovery maps for the thin-lip inlet, $M_\infty = 1.5$; $\alpha = 4^\circ$.



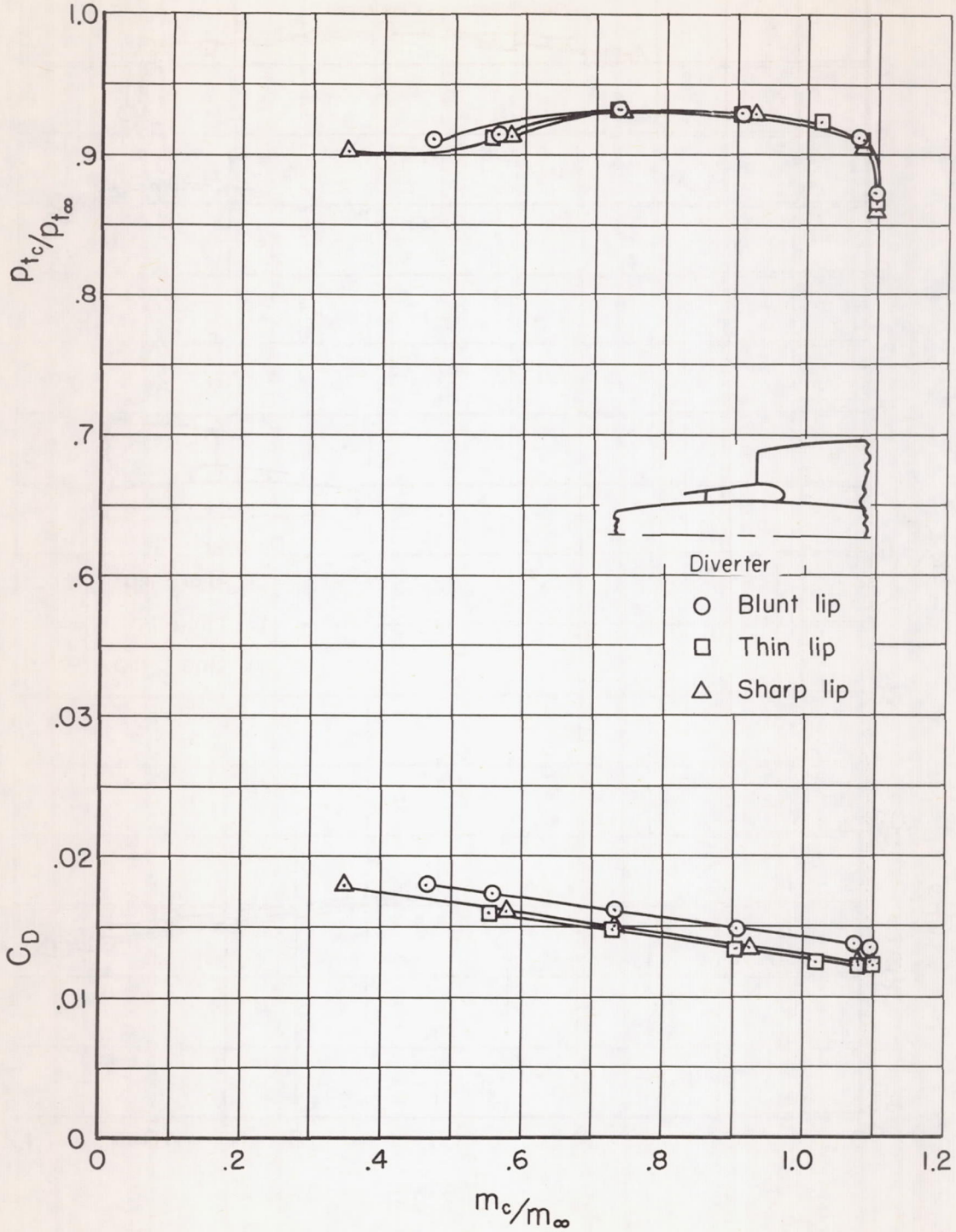
(a) $M_\infty = 0.9$

Figure 15.- The variation of total-pressure-recovery ratio and drag coefficient with mass-flow ratio for the three inlet lip shapes, $\alpha = 4^\circ$.



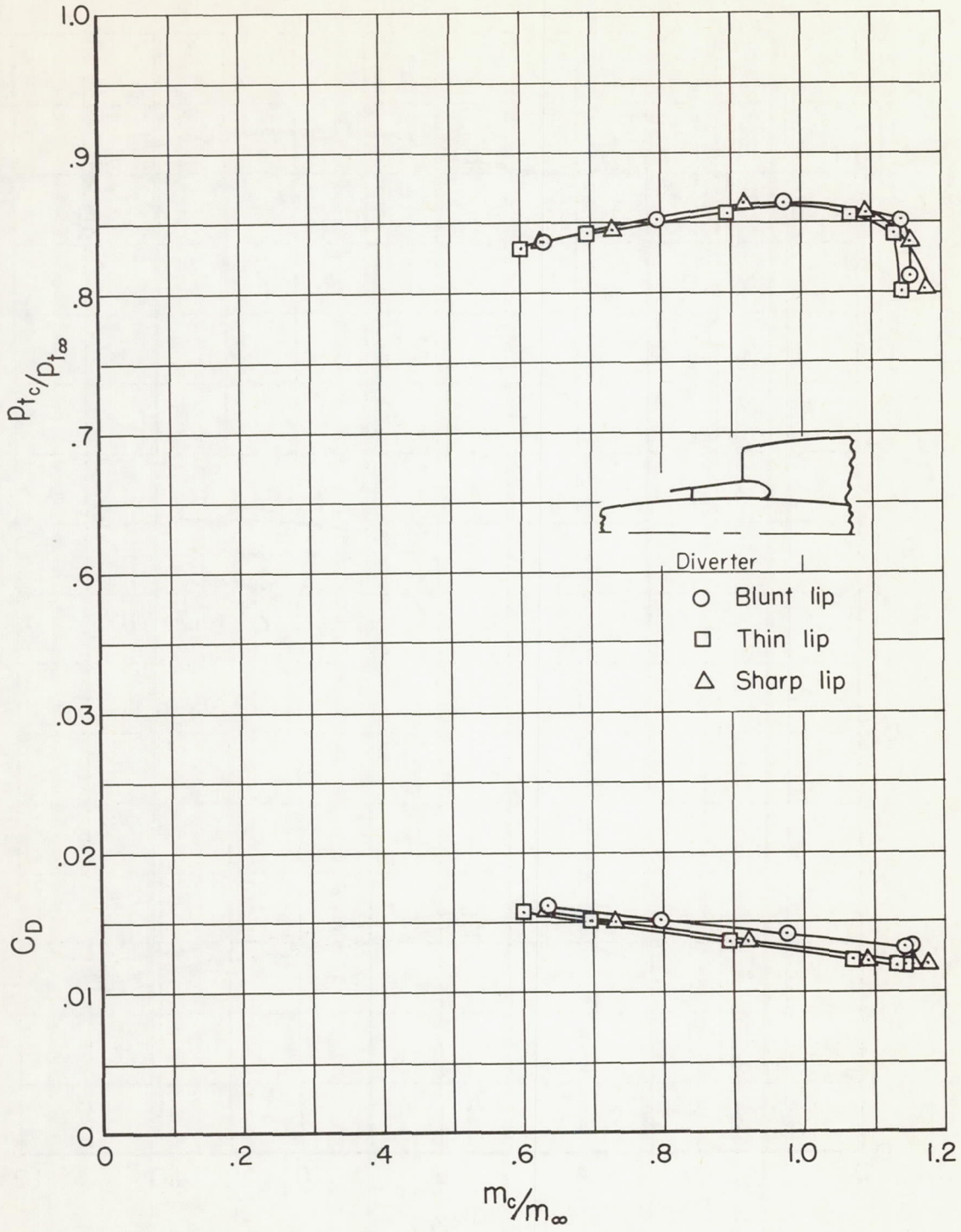
(b) $M_\infty = 1.3$

Figure 15.- Continued.



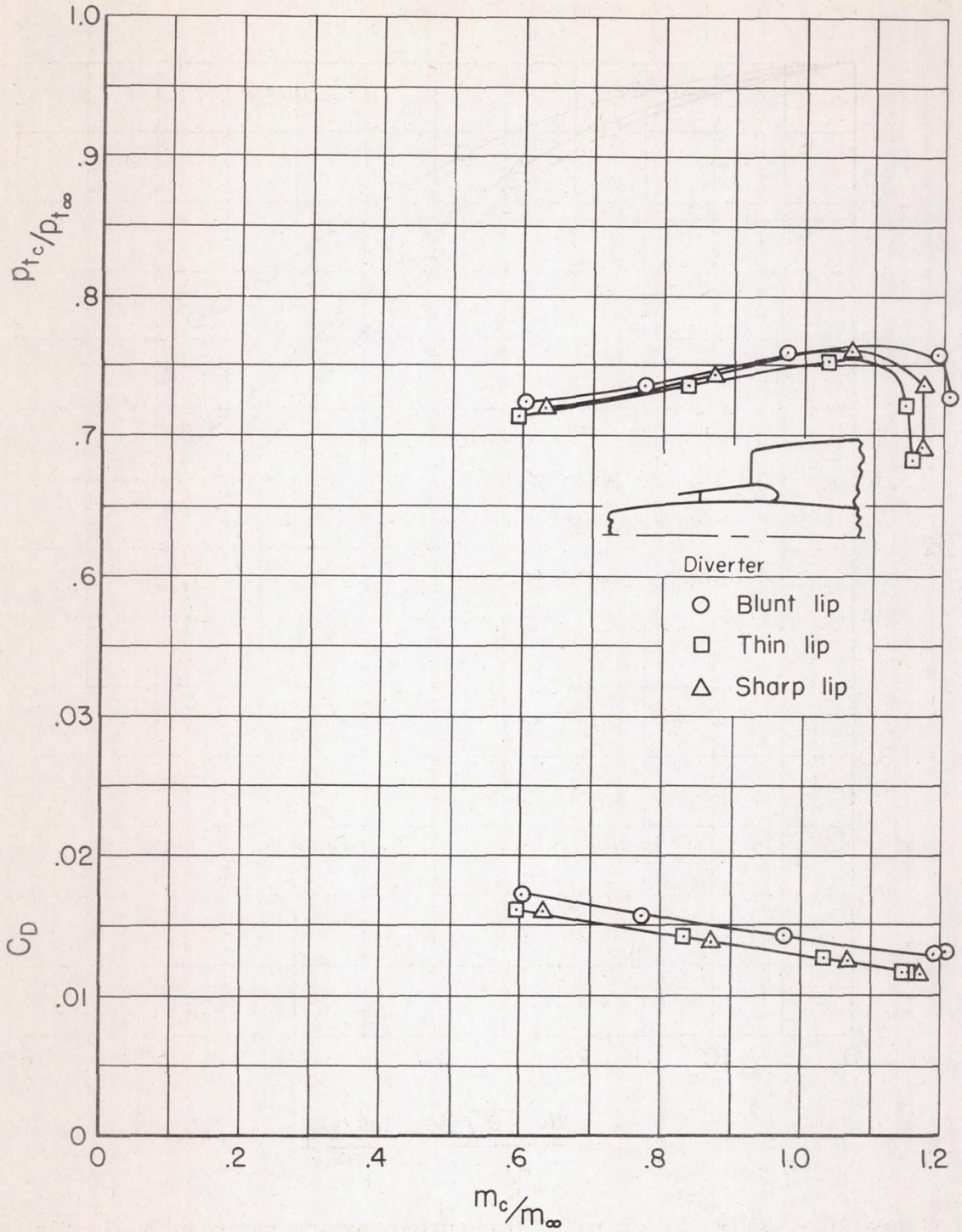
(c) $M_\infty = 1.5$

Figure 15.- Continued.



(d) $M_\infty = 1.7$

Figure 15.- Continued.



(e) $M_\infty = 1.9$

Figure 15.- Concluded.

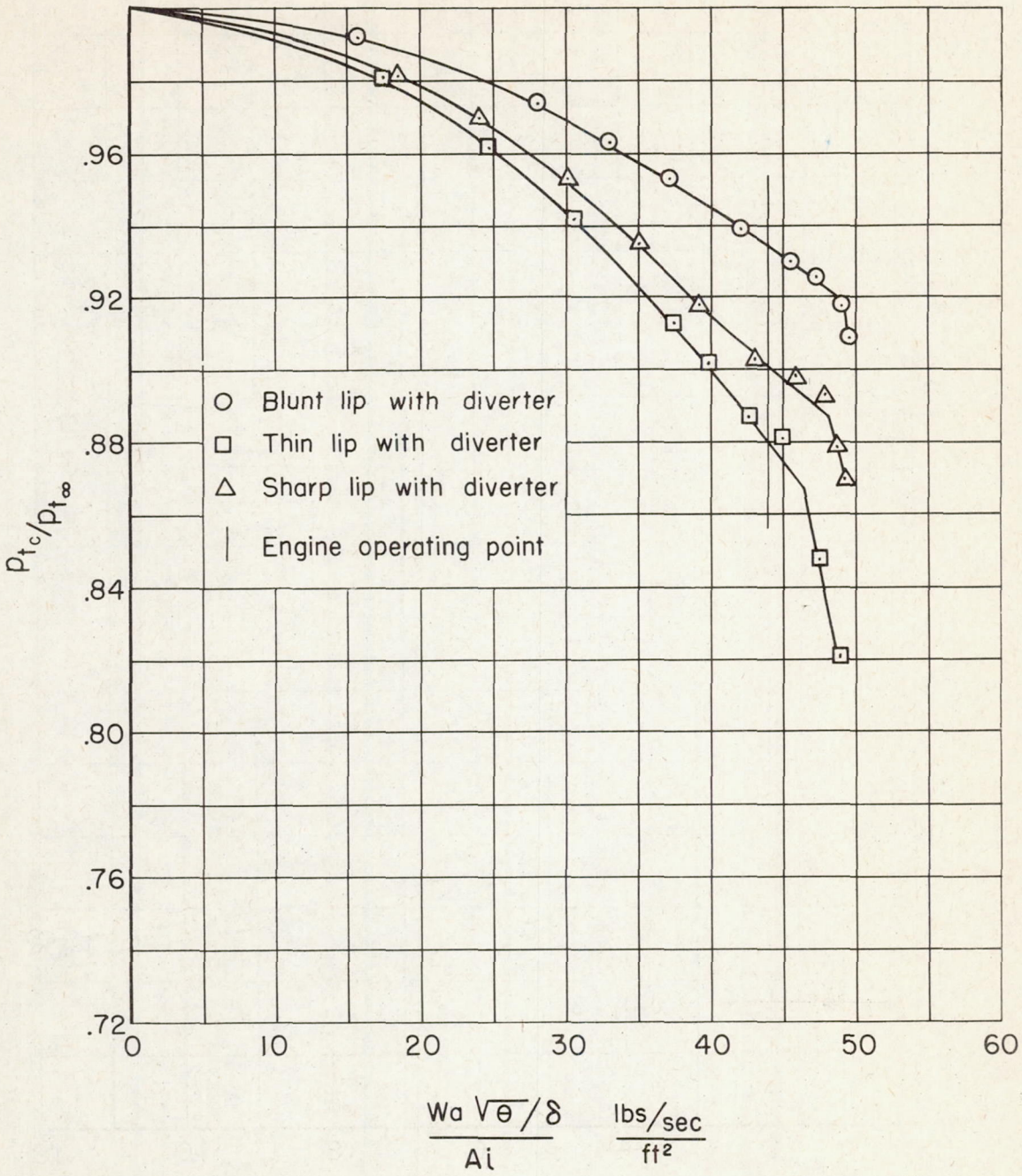


Figure 16.- Variation of total-pressure-recovery ratio with air-flow parameter for the static operating condition; $M_\infty = 0$, $A_i = 4.21$ square feet, JT-3C-20 engine.

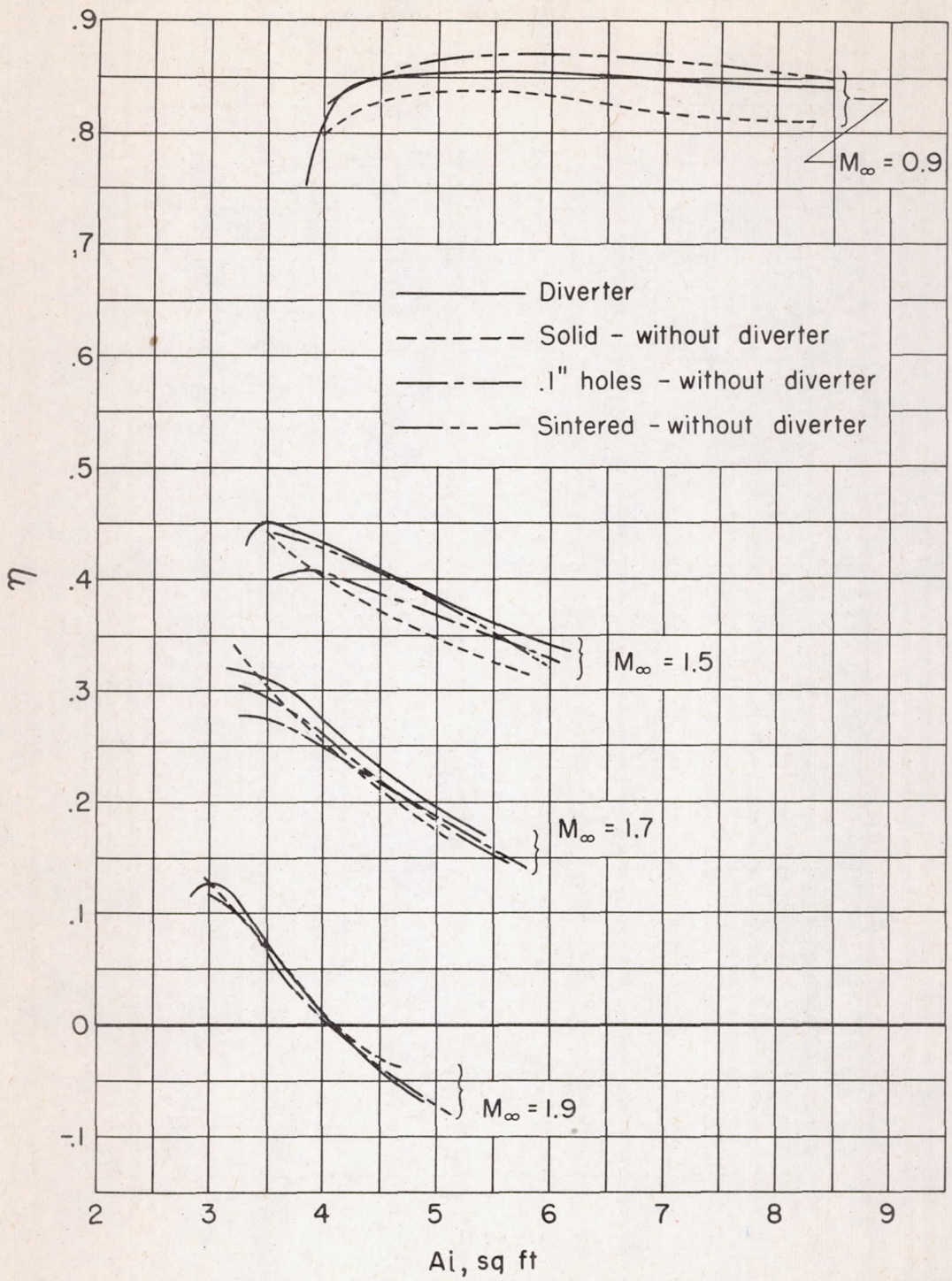


Figure 17.- Net thrust parameter as a function of inlet area for the thin-lip inlet configurations; altitude = 35,000 feet, JT-3C-20 engine.

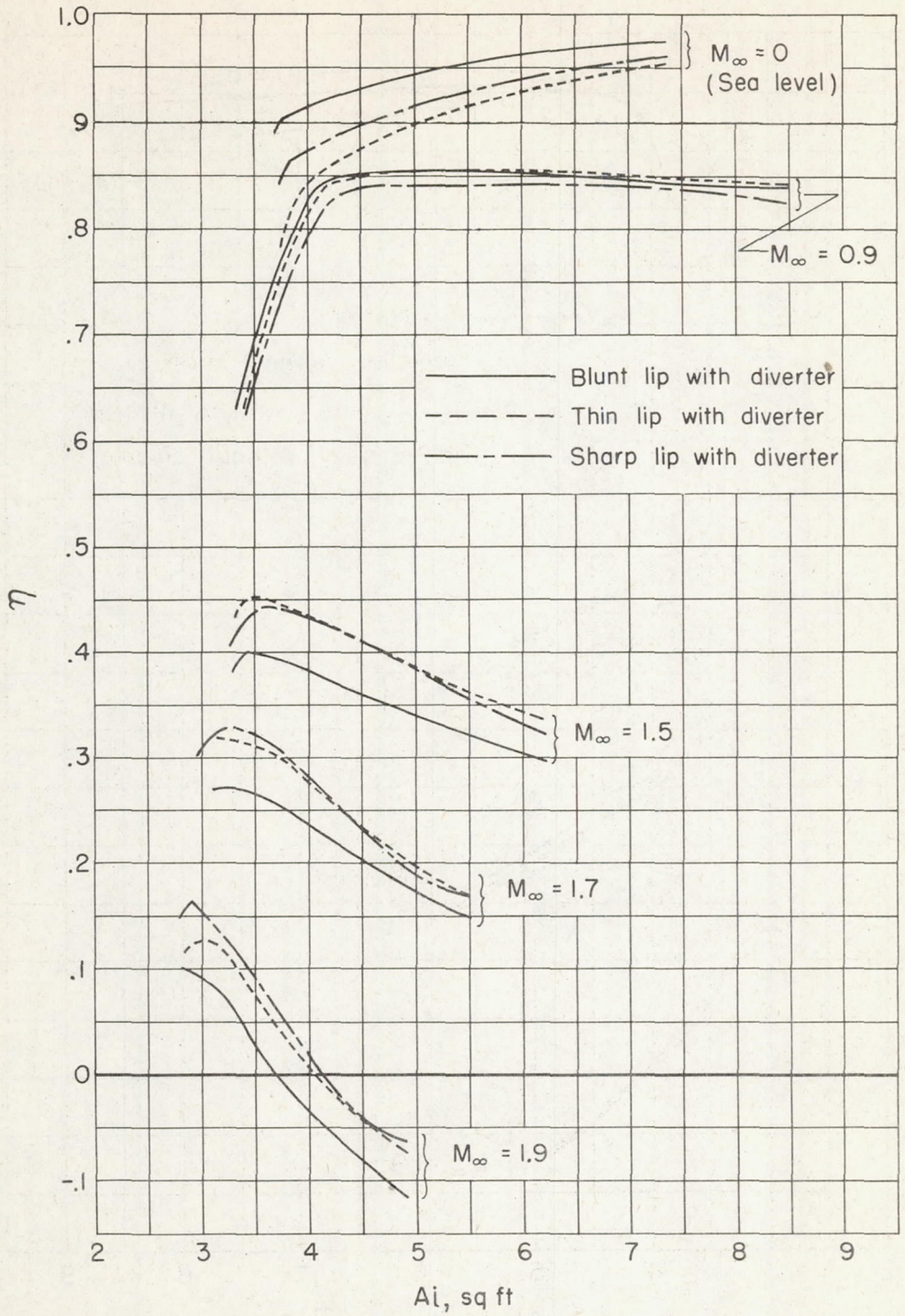


Figure 18.- Net thrust parameter as a function of inlet area for the three inlet lip shapes; altitude = 35,000 feet except as noted, JT-3C-20 engine.